TPM Vol. 32, No. S6, 2025
ISSN: 1972-6325
https://www.tpmap.org/

Open Access

INTRANASAL DELIVERY OF RESVERATROL AND PIPERINE NANOSTRUCTURED LIPID CARRIERS: SYNERGISTIC NEUROPROTECTION IN A 6-HYDROXYDOPAMINE-INDUCED PARKINSON'S DISEASE RAT MODEL

NEHA SAINI[1], NEETU PANWAR[2], MADHAV MOHAN[3], RITU KATARIA[4], DIMPY RANI[5*]

[1] G.D. GOENKA UNIVERSITY, SOHNA, GURUGRAM, INDIA (ORCID: 0009-0006-1484-4812)
[2] SCHOOL OF APPLIED SCIENCES, SHRI VENKATESHWARA UNIVERSITY, GAJRAULA, UP, INDIA (ORCID: 0000-0002-2401-7259)
[3] INSTITUTE OF PHARMACY, DOSUT, NALANDA (ORCID: 0009-0004-1347-6435)
[4] GVM COLLEGE OF PHARMACY, SONIPAT, HARYANA, INDIA (ORCID: 0009-0003-3614-9149)
[5] G.D. GOENKA UNIVERSITY, SOHNA, GURUGRAM, INDIA (ORCID: 0000-0003-4618-0177)

Abstract:
Parkinson's disease (PD) is a progressive neurodegenerative disorder characterized by dopaminergic neuronal loss, leading to motor and cognitive impairments. This study investigates the neuroprotective potential of intranasally delivered Resveratrol-loaded Nanostructured Lipid Carriers (R-NLC), Piperine-loaded NLC (P-NLC), and their combined formulation (R+P-NLC) in a 6-hydroxydopamine (6-OHDA)-induced PD rat model, compared to intravenous Levodopa. Male Wistar rats were subjected to unilateral 6-OHDA lesions in the substantia nigra or striatum, followed by twice-daily intranasal administration of NLC formulations for three weeks. Behavioral assessments, including Rotarod, Open Field, Grip Strength, Y-Maze, and Morris Water Maze tests, conducted on Days 7, 14, and 21, revealed significant improvements in motor coordination, locomotor activity, fine motor skills, and cognitive function in treated groups compared to the PD group. Biochemical analyses demonstrated restored dopamine levels, reduced glutamate and acetylcholine levels, and improved oxidative stress markers (MDA, SOD, GSH, CAT) in treated groups, with R+P-NLC and Levodopa showing superior efficacy. Histological analysis of the substantia nigra and striatum confirmed significant neuroprotection, with R+P-NLC exhibiting near-normal neuronal morphology, suggesting a synergistic effect of Resveratrol and Piperine. These findings highlight the potential of intranasal NLC delivery as an effective, non-invasive strategy for PD treatment, with the combined R+P-NLC formulation offering promising therapeutic benefits.
Keywords: Parkinson's disease, Intranasal delivery, Nanostructured Lipid Carriers, Resveratrol, Piperine

INTRODUCTION

Parkinson's disease (PD) is a progressive neurodegenerative disorder and the second most common neurodegenerative condition globally, affecting approximately 1–2% of individuals over 60, with an increasing prevalence in aging populations (Armstrong & Okun, 2020). Characterized by the loss of dopaminergic neurons in the substantia nigra pars compacta (SNpc) and the accumulation of α-synuclein aggregates in Lewy bodies, PD manifests through motor symptoms such as bradykinesia, rigidity, resting tremor, and postural instability, alongside non-motor symptoms including cognitive impairment, depression, and autonomic dysfunction (Bloem et al., 2021). The depletion of dopamine in the striatum, resulting from nigrostriatal dopaminergic degeneration, disrupts basal ganglia circuitry critical for motor control (Surmeier et al., 2023). Levodopa, a dopamine precursor, remains the cornerstone of PD treatment for alleviating motor symptoms. However, its long-term use is associated with complications such as dyskinesia, motor fluctuations, and limited efficacy against non-motor symptoms or disease progression (Armstrong & Okun, 2020).

The pathogenesis of PD is multifactorial, involving oxidative stress, mitochondrial dysfunction, excitotoxicity, and neuroinflammation, which collectively drive neuronal death (Simon et al., 2020). Oxidative stress, driven by reactive oxygen species (ROS) from dopamine metabolism and mitochondrial impairment, causes lipid peroxidation, protein misfolding, and DNA damage, exacerbating neurodegeneration (Blesa et al., 2022). Glutamate-mediated excitotoxicity and dysregulated cholinergic signaling further contribute to neuronal damage by promoting hyperexcitability and motor deficits (Liu, 2020). Consequently, there is an urgent need for novel therapies that target these mechanisms to provide neuroprotection and address both motor and non-motor symptoms of PD.

Resveratrol, a natural polyphenol found in grapes and red wine, has shown promise as a neuroprotective agent due to its antioxidant, anti-inflammatory, and anti-apoptotic properties (Gambini & Gimeno-Mallench, 2022). Recent studies have

demonstrated that Resveratrol mitigates oxidative stress, upregulates antioxidant enzymes such as superoxide dismutase (SOD) and catalase (CAT), and modulates neuroinflammatory pathways, protecting dopaminergic neurons in PD models (Liu et al., 2022). However, Resveratrol's clinical application is hindered by its poor water solubility, low bioavailability, and rapid systemic metabolism, which limit its ability to cross the blood-brain barrier (BBB) (Bilia et al., 2021). Piperine, an alkaloid from black pepper, enhances the bioavailability of co-administered drugs by inhibiting hepatic and intestinal metabolism, particularly via cytochrome P450 enzymes (Gorgani et al., 2021). Piperine also exhibits antioxidant and anti-inflammatory effects, making it a potential co-therapeutic for PD (Srinivasan, 2023). The combination of Resveratrol and Piperine may offer synergistic neuroprotection by enhancing bioavailability and targeting multiple PD-related pathways, but effective brain delivery remains a challenge.

The BBB restricts the passage of most therapeutic molecules into the central nervous system (CNS), limiting the efficacy of oral and systemic administration routes (Dong, 2021). Intranasal delivery has emerged as a non-invasive strategy to bypass the BBB, enabling direct nose-to-brain transport via the olfactory and trigeminal nerve pathways (Pires et al., 2022). This route facilitates rapid drug absorption through the nasal mucosa, achieving higher brain concentrations with reduced systemic exposure (Agrawal et al., 2020). However, challenges such as mucociliary clearance and limited nasal retention time necessitate advanced drug delivery systems to optimize intranasal administration.

Nanostructured Lipid Carriers (NLCs) are advanced lipid-based nanoparticles that offer high drug encapsulation efficiency, controlled release, and enhanced stability, making them ideal for intranasal delivery (Haider et al., 2020). Their small particle size (100–200 nm) facilitates mucosal penetration and brain targeting, while mucoadhesive modifications can prolong nasal retention (Khosa et al., 2021). Recent studies have demonstrated that NLCs effectively deliver neuroprotective agents to the brain, improving therapeutic outcomes in neurodegenerative disorders (Scioli Montoto et al., 2020). Incorporating Resveratrol and Piperine into NLCs for intranasal delivery could overcome their pharmacokinetic limitations, enhance brain bioavailability, and maximize neuroprotective effects in PD.

The 6-hydroxydopamine (6-OHDA) rat model is a well-established preclinical model for PD, replicating key pathological features such as dopaminergic neuronal loss, oxidative stress, and motor deficits through selective neurotoxicity (Zeng et al., 2023). This model is ideal for evaluating novel therapeutic strategies, as it allows assessment of both motor and non-motor symptoms and their response to treatment (Blandini & Armentero, 2022). In this study, we investigate the neuroprotective efficacy of intranasally delivered Resveratrol-loaded NLCs (R-NLC), Piperine-loaded NLCs (P-NLC), and their combined formulation (R+P-NLC) in a 6-OHDA-induced PD rat model, compared to intravenous Levodopa. Through comprehensive behavioral, biochemical, and histological analyses, we aim to elucidate the therapeutic potential of these NLC formulations, with a focus on their synergistic effects and the advantages of intranasal delivery for PD treatment.

2. MATERIALS AND METHODS

2.1 Experimental Design

This study evaluates the synergistic neuroprotective effects of intranasal resveratrol (RES) and piperine (PIP)-loaded nanostructured lipid carriers (NLCs) in a 6-hydroxydopamine (6-OHDA)-induced Parkinson's disease (PD) model in Wistar rats, compared to RES-alone NLCs, PIP-alone NLCs, L-DOPA-loaded NLCs, and control groups. The total study duration is 53 days (~8 weeks), comprising a 10-day pre-surgery phase (7 days acclimatization, 3 days baseline behavioral testing) and a 43-day post-surgery phase (Day 0: 6-OHDA lesioning; Days 1–42: daily intranasal treatment; Day 43: sacrifice and analyses). The design is randomized, controlled, and blinded at all stages—surgery, drug administration, behavioral, biochemical, histological, and pharmacokinetic assessments—to minimize bias, adhering to ARRIVE 2.0 guidelines (Percie du Sert et al., 2020). The unilateral 6-OHDA model targets the substantia nigra pars compacta (SNpc) and striatum to induce nigrostriatal degeneration, mimicking early- to mid-stage PD motor and cognitive deficits (Blandini & Armentero, 2022). Outcomes include motor function (rotarod, open field, grip strength, stepping tests), cognitive performance (Y-maze, Morris water maze [MWM]), oxidative stress markers (malondialdehyde [MDA], superoxide dismutase [SOD], glutathione [GSH], catalase [CAT]), neuroinflammatory markers (interleukin-1β [IL-1β], tumor necrosis factor-α [TNF-α]), neurotransmitter levels (dopamine, glutamate, acetylcholine), brain delivery (pharmacokinetics on Day 42, blood-brain barrier [BBB] penetration on Day 14), histological changes (tyrosine hydroxylase [TH] staining), and nasal tolerability. Wistar rats were selected for their reproducible PD-like symptoms in the 6-OHDA model (Jin et al., 2008; Shrivastava et al., 2013). The 6-week treatment duration (Days 1–42) balances chronic neuroprotection assessment with ethical minimization of animal distress, supported by studies showing significant effects within 4–8 weeks (Sharma et al., 2016; Wen et al., 2024).

2.2 Experimental Animals

Adult male Wistar rats (8–10 weeks old, body weight 200–250 g) were sourced from a CPCSEA-registered breeding facility. Rats were housed in polycarbonate cages (4 rats per cage, 43 × 27 × 15 cm) under controlled environmental conditions: temperature (22 ± 2°C), relative humidity (55 ± 5%), and a 12-hour light/dark cycle. Animals had ad libitum access to standard rodent chow (Nutrimix Std-1020, Provimi, India) and filtered water. Bedding consisted of autoclaved corn cob, changed twice weekly to maintain hygiene. All experimental procedures were approved by the Institutional Animal Ethics Committee (IAEC) under CPCSEA Registration No. 129/PO/RES/09/CPCSEA, in compliance with CPCSEA guidelines, and adhered to the ARRIVE 2.0 guidelines for transparent reporting of animal research (Percie du Sert et al., 2020). A total of 42 rats were used, randomly assigned to seven groups (n = 6 per group), based on power calculations (80% power, $\alpha = 0.05$) to detect significant differences in neurobehavioral outcomes (Festing, 2018).

Randomization was performed using a random number generator, and group assignments were blinded to experimenters conducting behavioral, biochemical, and histological assessments to minimize bias.

2.2 Chemicals and Reagents

All chemicals were analytical grade to ensure purity and reproducibility. Resveratrol (≥99%, Cat. No. R5010), 6-OHDA hydrobromide (Cat. No. H4381), L-DOPA (≥98%, Cat. No. D9628), and rhodamine B (Cat. No. R6626) were procured from Sigma-Aldrich (St. Louis, MO, USA) for neuroprotection, lesion induction and motor restoration, respectively (Jin et al., 2008; Sharma et al., 2016; Pardeshi & Belgamwar, 2019). Piperine (≥98%, Cat. No. 11639) was sourced from Cayman Chemical (Ann Arbor, MI, USA) for its anti-inflammatory and bioenhancer properties (Shrivastava et al., 2013). Lipid components included glyceryl monostearate (Imwitor® 900K) and oleic acid (Kollicream® OA) from Gattefossé (Saint-Priest, France) for NLC formulation (Bhalekar et al., 2017). Surfactants (Poloxamer 188 [Kolliphor® P188], Tween 80), ascorbic acid, saline, dialysis bags (MWCO 12–14 kDa), o-phthalaldehyde, and HPLC-grade solvents (methanol, potassium dihydrogen phosphate) were obtained from Thermo Fisher Scientific (Waltham, MA, USA) for analytical compatibility (Wen et al., 2024).

2.3 Equipment

Advanced equipment ensured precision and reproducibility. NLCs were prepared using a high-pressure homogenizer (PandaPLUS 2000, GEA Niro Soavi, Italy) and a probe sonicator (Sonics Vibra-Cell VCX 750, Newtown, CT, USA; 20 kHz) for nanoscale particles (Bhalekar et al., 2017). Particle characteristics were measured with a Zetasizer Nano ZS (Malvern Panalytical, UK). HPLC (Agilent 1260 Infinity II, USA) with electrochemical (ECD) and fluorescence detectors quantified drugs and neurotransmitters (Liu, 2020). Stereotaxic surgery used a Model 51730 apparatus (Stoelting Co., USA). Behavioral assessments employed a rotarod (Ugo Basile, Italy), grip strength meter (Columbus Instruments, USA), and EthoVision XT software (Noldus, Netherlands). Histological analysis utilized a microtome (Leica RM2255), cryostat (Leica CM3050 S), Leica Bond Polymer Refine Detection kit, and Nikon Eclipse Ti2 fluorescence microscope (Japan). Intranasal administration used an Eppendorf Research Plus micropipette (0.5–10 µL) with PE10 tubing (Braintree Scientific, USA). In vitro release studies used a shaking incubator (LabTech LSI-3016R, Daihan Labtech, South Korea), and biochemical assays employed a Bio-Rad microplate reader and Polytron PT 3100 homogenizer (Kinematica, Switzerland).

2.4 Preparation of Nanostructured Lipid Carriers (NLCs)

2.4.1 Resveratrol and Piperine-Loaded NLCs (RES-PIP-NLCs)

RES-PIP-NLCs were prepared using the melt emulsification-probe sonication method, as described by Bhalekar et al. (2017). The lipid phase, consisting of glyceryl monostearate (70% w/w) and oleic acid (30% w/w), was melted at 70°C. Resveratrol (10 mg) and piperine (5 mg) were dissolved in the lipid phase at a 2:1 RES:PIP ratio, optimized for synergistic antioxidant effects based on in vitro studies (Singh & Pai, 2015). These quantities were used for a batch sufficient to prepare multiple doses, with the final NLC suspension diluted to deliver in vivo doses of 10 mg/kg RES and 2.5 mg/kg PIP. The aqueous phase, containing Poloxamer 188 (1.5% w/v) and Tween 80 (0.5% w/v) in distilled water, was heated to 70°C. The lipid phase was emulsified into the aqueous phase using a high-speed homogenizer (10,000 rpm, 5 min), followed by probe sonication (20 kHz, 40% amplitude, 10 min) to achieve nanoscale particles. The nanoemulsion was cooled to 25°C, forming NLCs. Particle size, polydispersity index (PDI), and zeta potential were measured using a Zetasizer Nano ZS. Drug loading and entrapment efficiency were quantified via HPLC (C18 column, methanol:water 70:30 v/v, 1 mL/min, UV detection at 306 nm for RES and 343 nm for PIP), following Pardeshi and Belgamwar (2019). The optimized RES-PIP-NLCs exhibited a particle size of 130 ± 15 nm, PDI of 0.160 ± 0.005, zeta potential of −25 ± 5 mV, drug loading of 12 ± 2% (RES) and 3 ± 1% (PIP), and entrapment efficiency of 75 ± 5% (RES) and 80 ± 4% (PIP). The NLC suspension was diluted to deliver 10 mg/kg RES (e.g., 2 mg for a 200 g rat) and 2.5 mg/kg PIP (e.g., 0.5 mg for a 200 g rat) in 20 µL per dose.

2.4.2 L-DOPA-Loaded Nanostructured Lipid Carriers (L-DOPA-NLCs)

L-DOPA-NLCs were prepared using the melt emulsification-probe sonication method, adapted from Sharma et al. (2016). The lipid phase, consisting of glyceryl monostearate (70% w/w) and oleic acid (30% w/w), was melted at 70°C. L-DOPA (10 mg) was dissolved in the lipid phase, ensuring solubility within the lipid matrix, as validated by Sharma et al. (2016). This quantity was used for a batch sufficient to prepare multiple doses, with the final NLC suspension diluted to deliver an in vivo dose of 10 mg/kg L-DOPA. The aqueous phase, containing Poloxamer 188 (1.5% w/v) and Tween 80 (0.5% w/v) in distilled water, was heated to 70°C. The lipid phase was emulsified into the aqueous phase using a high-speed homogenizer (10,000 rpm, 5 min), followed by probe sonication (20 kHz, 40% amplitude, 8 min) to achieve nanoscale particles. The nanoemulsion was cooled to 25°C, forming NLCs. Particle size, PDI, and zeta potential were measured using a Zetasizer Nano ZS. Drug loading and entrapment efficiency were quantified via HPLC (C18 column, 0.1 M potassium dihydrogen phosphate buffer:methanol 85:15 v/v, pH 3.0, 1 mL/min, UV detection at 280 nm), as described by Sharma et al. (2016). The optimized L-DOPA-NLCs exhibited a particle size of 140 ± 20 nm, PDI of 0.180 ± 0.010, zeta potential of −22 ± 4 mV, drug loading of 10 ± 2%, and entrapment efficiency of 70 ± 5%. The NLC suspension was diluted to deliver 10 mg/kg L-DOPA (e.g., 2 mg for a 200 g rat) in 20 µL per dose.

2.4.3 Resveratrol-Loaded NLCs (RES-NLCs)

RES-NLCs were prepared using the melt emulsification-probe sonication method, adapted from Bhalekar et al. (2017). The lipid phase, consisting of glyceryl monostearate (70% w/w) and oleic acid (30% w/w), was melted at 70°C. Resveratrol (10 mg) was dissolved in the lipid phase, ensuring solubility within the lipid matrix. This quantity was used for a batch sufficient to prepare multiple doses, with the final NLC suspension diluted to deliver an in vivo dose of 10 mg/kg RES. The aqueous phase, containing Poloxamer 188 (1.5% w/v) and Tween 80 (0.5% w/v) in distilled water, was

heated to 70°C. The lipid phase was emulsified into the aqueous phase using a high-speed homogenizer (10,000 rpm, 5 min), followed by probe sonication (20 kHz, 40% amplitude, 8 min) to achieve nanoscale particles. The nanoemulsion was cooled to 25°C, forming NLCs. Particle size, PDI, and zeta potential were measured using a Zetasizer Nano ZS. Drug loading and entrapment efficiency were quantified via HPLC (C18 column, methanol:water 70:30 v/v, 1 mL/min, UV detection at 306 nm), as described by Pardeshi and Belgamwar (2019). The optimized RES-NLCs exhibited a particle size of 135 ± 15 nm, PDI of 0.170 ± 0.008, zeta potential of −24 ± 5 mV, drug loading of 12 ± 2%, and entrapment efficiency of 75 ± 5%. NLC suspensions were stored at 4°C, protected from light, and used within 7 days, with stability confirmed via particle size and drug content analysis (no significant change, $p > 0.05$). In vitro drug release was assessed using a dialysis bag method (MWCO 12–14 kDa, phosphate buffer pH 6.8, 34°C, 100 rpm), showing 65 ± 5% RES release over 24 hours, as per Sharma et al. (2016). The NLC suspension was diluted to deliver 10 mg/kg RES (e.g., 2 mg for a 200 g rat) in 20 µL per dose.

2.4.4 Piperine-Loaded Nanostructured Lipid Carriers (PIP-NLCs)

PIP-NLCs were prepared using the melt emulsification-probe sonication method, adapted from Bhalekar et al. (2017). The lipid phase, consisting of glyceryl monostearate (70% w/w) and oleic acid (30% w/w), was melted at 70°C. Piperine (5 mg) was dissolved in the lipid phase, ensuring solubility within the lipid matrix. This quantity was used for a batch sufficient to prepare multiple doses, with the final NLC suspension diluted to deliver an in vivo dose of 2.5 mg/kg PIP. The aqueous phase, containing Poloxamer 188 (1.5% w/v) and Tween 80 (0.5% w/v) in distilled water, was heated to 70°C. The lipid phase was emulsified into the aqueous phase using a high-speed homogenizer (10,000 rpm, 5 min), followed by probe sonication (20 kHz, 40% amplitude, 8 min) to achieve nanoscale particles. The nanoemulsion was cooled to 25°C, forming NLCs. Particle size, PDI, and zeta potential were measured using a Zetasizer Nano ZS. Drug loading and entrapment efficiency were quantified via HPLC (C18 column, methanol:water 70:30 v/v, 1 mL/min, UV detection at 343 nm), as described by Pardeshi and Belgamwar (2019). The optimized PIP-NLCs exhibited a particle size of 132 ± 15 nm, PDI of 0.165 ± 0.007, zeta potential of −24 ± 5 mV, drug loading of 3 ± 1%, and entrapment efficiency of 80 ± 4%. NLC suspensions were stored at 4°C, protected from light, and used within 7 days, with stability confirmed via particle size and drug content analysis (no significant change, $p > 0.05$). In vitro drug release was assessed using a dialysis bag method (MWCO 12–14 kDa, phosphate buffer pH 6.8, 34°C, 100 rpm), showing 70 ± 4% PIP release over 24 hours, as per Sharma et al. (2016). The NLC suspension was diluted to deliver 2.5 mg/kg PIP (e.g., 0.5 mg for a 200 g rat) in 20 µL per dose.

2.5 6-OHDA-Induced Parkinson's Disease Model

On Day 0, a unilateral 6-hydroxydopamine (6-OHDA) lesion was induced in the substantia nigra pars compacta (SNpc) and striatum of Wistar rats (except the control group) to establish a Parkinson's disease (PD) model, mimicking nigrostriatal degeneration characteristic of early- to mid-stage PD (Blandini & Armentero, 2022). Rats were anesthetized with ketamine (80 mg/kg, intraperitoneal [i.p.]) and xylazine (10 mg/kg, i.p.), achieving deep anesthesia, confirmed by the absence of a toe-pinch reflex, to ensure humane surgical conditions without respiratory compromise. Each rat was secured in a stereotaxic frame (Model 51730, Stoelting Co., USA) with ear bars and a bite bar to align the skull at bregma, ensuring precise targeting. A midline incision (1.5 cm) was made on the scalp to expose the skull, and two burr holes (0.8 mm diameter) were drilled using a dental drill to access the right substantia nigra pars compacta (SNpc) and striatum, key regions of the nigrostriatal pathway affected in PD (Blesa et al., 2022). Stereotaxic coordinates, based on the rat brain atlas (Paxinos & Watson, 2007), were: substantia nigra (anteroposterior [AP]: −5.3 mm, mediolateral [ML]: +2.0 mm, dorsoventral [DV]: −7.8 mm from bregma); striatum (AP: +0.5 mm, ML: +3.0 mm, DV: −5.0 mm from bregma). These coordinates ensure accurate targeting of dopaminergic neurons in the SNpc and their projections in the striatum, critical for inducing PD-like motor and cognitive deficits (Jin et al., 2008). 6-OHDA hydrobromide (2.5 µg/1 µL per site, total 5 µg/2 µL in 0.1% ascorbic acid-saline to prevent oxidation) was injected into each region at a rate of 0.5 µL/min using a 10 µL Hamilton syringe fitted with a 26-gauge needle, controlled by a microinfusion pump (Harvard Apparatus, USA). The lower dose per site (2.5 µg) compared to single-site lesioning accounts for the dual-target approach, ensuring sufficient dopamine depletion (>50%) while minimizing non-specific damage, as validated in prior studies (Shrivastava et al., 2013). The needle remained in place for 5 minutes post-injection at each site to prevent backflow, ensuring precise delivery of the neurotoxin. The control and sham groups received vehicle injections (1 µL 0.1% ascorbic acid-saline per site, total 2 µL) at the same coordinates to control for surgical effects. Following injections, the scalp was sutured with 4-0 nylon, and buprenorphine (0.05 mg/kg, subcutaneous [s.c.]) was administered for post-operative analgesia to minimize discomfort. Rats were placed in a heated recovery cage (30°C) and monitored for recovery of the righting reflex and feeding behavior within 4 hours, with daily checks for signs of infection, distress, or weight loss (>10%) to ensure animal welfare (JoVE, 2021).

2.6 Experimental Groups and Treatment

Forty-two rats were randomly assigned to seven groups (n = 6/group) post-acclimatization (Day -4). Groups were:

(1) Control (intranasal saline, 20 µL)
(2) Sham (vehicle injection + saline, 20 µL)
(3) 6-OHDA (6-OHDA + saline, 20 µL)
(4) RES-NLC (6-OHDA + RES-NLCs, 10 mg/kg RES in 20 µL)
(5) PIP-NLC (6-OHDA + PIP-NLCs, 2.5 mg/kg PIP in 20 µL)
(6) RES-PIP-NLC (6-OHDA + RES-PIP-NLCs, 10 mg/kg RES + 2.5 mg/kg PIP in 20 µL)
(7) Standard (6-OHDA + L-DOPA-NLCs, 10 mg/kg L-DOPA in 20 µL).

.6.1 Dosage Selection Rationale

The resveratrol dose (10 mg/kg) was selected based on its proven neuroprotective efficacy in 6-OHDA-induced PD models in Wistar rats. Jin et al. (2008) demonstrated that resveratrol at 10–20 mg/kg (i.p.) significantly improved motor function and reduced oxidative stress, with 10 mg/kg achieving optimal efficacy without adverse effects. The intranasal route enhances brain bioavailability by bypassing the blood-brain barrier (BBB), as validated by Wen et al. (2024), justifying the 10 mg/kg dose for NLC formulations to achieve therapeutic brain concentrations while maintaining solubility within the lipid matrix (Pardeshi & Belgamwar, 2019). The piperine dose (2.5 mg/kg) was chosen for its dual role as a neuroprotective agent and bioenhancer. Shrivastava et al. (2013) reported that piperine at 2.5–10 mg/kg (oral) reduced oxidative stress and apoptosis in 6-OHDA-treated Wistar rats, with 2.5 mg/kg being effective and safe. Piperine's inhibition of CYP3A4 and P-glycoprotein enhances resveratrol's bioavailability, as shown in pharmacokinetic studies (Singh & Pai, 2015). The 2.5 mg/kg dose minimizes potential gastrointestinal irritation observed at higher doses (>10 mg/kg) in rats (Baspinar et al., 2018), ensuring safety for chronic intranasal administration. The L-DOPA dose (10 mg/kg) was selected based on its established efficacy in 6-OHDA rat models, improving motor function and dopamine levels when delivered intranasally via NLCs, as validated by Sharma et al. (2016) and Wen et al. (2024). The dose is feasible for intranasal administration in 20 µL, ensuring consistency with other groups.

2.6.2 Administration Method

Treatments were administered intranasally daily for 10 weeks, starting 24 hours post-6-OHDA injection (or vehicle for control/sham groups), to target early neurodegeneration. All formulations were delivered as liquid solutions (20 µL total, 10 µL per nostril) using a micropipette (Eppendorf Research Plus, 0.5–10 µL) with a soft polyethylene catheter (PE10 tubing, Braintree Scientific, USA), as described by Wen et al. (2024). The RES-PIP-NLC group received a liquid NLC suspension containing 10 mg/kg RES (e.g., 2 mg for a 200 g rat) and 2.5 mg/kg PIP (e.g., 0.5 mg for a 200 g rat) in 20 µL, adjusted for body weight. The standard group received L-DOPA-NLCs containing 10 mg/kg L-DOPA (e.g., 2 mg for a 200 g rat) in 20 µL, adjusted for body weight. The 20 µL volume was selected to prevent nasal overflow, consistent with standard intranasal dosing in Wistar rats (Wen et al., 2024). Rats were lightly anesthetized with isoflurane (2%, 1 min) during administration to ensure precise delivery and minimize stress, as per JoVE (2021). The liquid NLC suspensions were chosen as they effectively deliver RES, PIP, and L-DOPA to the brain via intranasal administration, leveraging the NLCs' nanoscale size and lipid matrix to enhance solubility and BBB penetration (Pardeshi & Belgamwar, 2019; Sharma et al., 2016; Wen et al., 2024).

2.7 Pharmacokinetic Analysis

On Day 42, a subset (n = 2/group, 14 rats) received a single intranasal dose of RES-NLCs, PIP-NLCs, RES-PIP-NLCs, or L-DOPA-NLCs and was sacrificed to assess steady-state pharmacokinetics after 6 weeks of dosing. Blood (1 mL) was collected via cardiac puncture under anesthesia (ketamine 80 mg/kg, xylazine 10 mg/kg, i.p.) at 1- and 4-hours post-dose. Plasma was separated (3,000 × g, 10 min, 4°C), and the striatum and substantia nigra were homogenized in 0.1 M perchloric acid with 0.01% EDTA. RES, PIP, and L-DOPA were quantified via HPLC (Agilent 1260 Infinity II, C18 column): RES and PIP (methanol:water 70:30 v/v, 1 mL/min, UV at 306 nm and 343 nm); L-DOPA (0.1 M phosphate buffer:methanol 85:15 v/v, pH 3.0, 1 mL/min, UV at 280 nm). Concentrations (ng/g tissue, ng/mL plasma) were calculated using standard curves (5–500 ng/mL, $R^2 > 0.99$; Wen et al., 2024).

2.8 Nasal Tolerability

On Day 43, nasal mucosa from 28 rats (n = 4/group) was collected post-sacrifice under anesthesia (ketamine 80 mg/kg, xylazine 10 mg/kg, i.p.). The nasal cavity was dissected, and mucosa was fixed in 4% paraformaldehyde (pH 7.4) for 24 hours at 4°C. Tissues were decalcified in 10% EDTA (pH 7.4) for 7–10 days, with daily solution changes. Decalcified tissues were embedded in paraffin, and 5 µm sections were cut using a Leica RM2255 microtome. Sections were deparaffinized in xylene (two changes, 5 min each), rehydrated through a graded ethanol series (100%, 95%, 70%, 5 min each), and stained with hematoxylin (Sigma-Aldrich, Cat. No. H3136) for 5 minutes to label nuclei, followed by rinsing in tap water for 5 minutes. Sections were counterstained with eosin (Sigma-Aldrich, Cat. No. E4009) for 2 minutes to visualize cytoplasm and extracellular matrix, rinsed in distilled water, and dehydrated (ethanol series: 70%, 95%, 100%, 2 min each). Slides were cleared in xylene, mounted with DPX mountant (Sigma-Aldrich, Cat. No. 06522), and examined under a Leica DM2500 microscope at 20x and 40x magnification. Histopathological changes (inflammation, epithelial damage, mucosal thickening) were scored semi-quantitatively (0 = none, 1 = mild, 2 = moderate, 3 = severe) by two blinded observers (Wen et al., 2024).

2.9 Behavioral Assessments

All behavioral assessments were conducted to evaluate motor coordination, locomotion, anxiety-like behavior, grip strength, forelimb akinesia, and cognitive function in the rats. Testing occurred on Days 14 (n = 6 rats/group; total 42 rats), 28, and 42 (n = 4 rats/group; total 28 rats) post-intervention, with baseline assessments performed on Days -3 to -1 to confirm equivalence across groups (one-way ANOVA, $p > 0.05$ for all measures). To minimize circadian influences and environmental variability, tests were carried out between 9:00 AM and 3:00 PM in a sound-attenuated room under controlled conditions (40 lux illumination, background noise <50 dB). All assessments were performed by observers blinded to group assignments. Prior to baseline testing, rats were acclimatized to the testing environment for 1 hour per day over 3 consecutive days.

2.9.1 Rotarod Test

The accelerating rotarod test (Ugo Basile, Varese, Italy) served as a primary measure for assessing motor coordination, balance, and endurance, which are critical indicators of cerebellar and basal ganglia function often impaired in neurodegenerative models. The apparatus consisted of a horizontally oriented, 7-cm-diameter knurled rod (to provide adequate grip without slippage) mounted approximately 30 cm above a cushioned platform to prevent injury upon falling.

Each rat was gently placed on the rod facing away from the direction of rotation to encourage forward walking. The rod was programmed to start at an initial speed of 4 revolutions per minute (rpm) and accelerate progressively to 40 rpm over a 5-minute trial duration, corresponding to an acceleration rate of approximately 7.2 rpm per minute, as commonly used in rodent protocols to challenge motor adaptability gradually. Latency to fall was automatically recorded in seconds using built-in infrared sensors that detected when the rat fell off the rod or completed a full passive rotation (indicating loss of active grip and coordination). Each testing session included three consecutive trials with a 5-minute inter-trial interval to allow recovery from muscular fatigue and prevent carryover effects, and the average latency across these trials was calculated for analysis. In healthy adult rats, typical latency values range from 100 to 300 seconds, with deficits often reducing this to below 100 seconds, as validated in studies demonstrating sensitivity to dopaminergic impairments in Parkinson's models (Zeng et al., 2023; calibration studies show inter-laboratory variability, but standardized acceleration yields reproducible results across setups).

2.9.2 Open Field Test

The open field test was utilized to quantify spontaneous locomotor activity and anxiety-like behavior, providing insights into exploratory tendencies, thigmotaxis (wall-hugging behavior), and overall emotional reactivity. The apparatus was a square arena measuring 100 cm × 100 cm × 40 cm, constructed from opaque black Plexiglas walls to block external visual cues and maintain uniform testing conditions. Rats were individually placed in the center of the arena and allowed unrestricted exploration for a 5-minute duration, a standard timeframe that captures initial exploratory activity without significant habituation. Key parameters included the total distance traveled (in centimeters, typically ranging from 2000 to 4000 cm in healthy control rats over 5 minutes), serving as an index of general locomotor activity, and the time spent in the central zone (defined as the inner 3 × 3 grid of nine equal squares, each approximately 33.3 cm × 33.3 cm, comprising about 11% of the total area), which inversely correlates with anxiety levels (reduced center time, e.g., <50 seconds, indicates heightened anxiety due to preference for peripheral zones). Additional metrics such as average velocity (in cm/s) and number of zone entries were also recorded. Behavioral trajectories were captured via an overhead camera and automatically analyzed using EthoVision XT software (Noldus Information Technology, Wageningen, Netherlands), which employs precise tracking algorithms for movement quantification. This protocol is validated for detecting locomotor hypoactivity and anxiety in neurodegenerative models, with arena sizes commonly standardized at 50-100 cm for rats to ensure scalability (Simon et al., 2020; studies confirm that distance traveled decreases with anxiety or motor deficits, while center time reflects emotional state).

2.9.3 Grip Strength Test

Forelimb grip strength was measured using a grip strength meter (Columbus Instruments, Columbus, OH, USA) to evaluate neuromuscular integrity, muscle power, and potential deficits in motor pathways. The apparatus featured a triangular wire grid (dimensions: approximately 10 cm wide with 0.2 cm wire diameter) connected to a sensitive digital force transducer capable of sampling at 1000 Hz for high-resolution force detection. The procedure involved positioning the rat such that its forepaws grasped the grid, followed by a steady horizontal pull on the tail at a constant speed of about 5 cm/s until the grip was released, with the peak force exerted (in grams) automatically recorded. Each rat performed three trials per forelimb (alternating left and right to avoid bias), with a 1-minute rest interval between trials to prevent fatigue, and the maximum force from each trial was averaged to obtain a reliable value per forelimb, enabling detection of bilateral or unilateral asymmetries. The measurement range of the transducer was 0-50 N (equivalent to 0-5 kgf), but typical peak force values in healthy adult Wistar rats range from 200 to 400 grams, with reductions indicating neuromuscular impairments. This test is non-invasive and highly repeatable, validated for screening motor deficits in models like Parkinson's disease (Blesa et al., 2022; protocols emphasize peak force as the primary metric, with grasp duration around 1 second in controls).

2.9.4 Stepping Test

The stepping test quantified forelimb akinesia, bradykinesia, and sensorimotor integration, particularly sensitive to nigrostriatal dopaminergic deficits. In the protocol, an experimenter restrained the rat by immobilizing its hindlimbs and one forelimb while supporting the torso, leaving the opposite forelimb free to contact a flat, non-slippery surface. The rat was then slowly dragged forward over a 90 cm distance at a controlled speed of approximately 18 cm/s (taking about 5 seconds), during which the number of adjusting steps—defined as deliberate paw placements to maintain balance and forward propulsion—was manually counted over a 10-second observation period to capture steady-state performance. The test was repeated three times per forelimb side (left and right), with at least 30 seconds between repetitions to reset posture, and the average number of steps per side was calculated, with asymmetries indicating lateralized impairments. In healthy control rats, typical adjusting step counts range from 10 to 15 per side in the 10-second window, while deficits (e.g., from MPTP treatment) significantly reduce this number, often leading to dragging rather than stepping. This simple test requires minimal equipment and is validated for unilateral motor assessments in Parkinson's models (Zeng et al., 2023; studies confirm persistent reductions in steps post-lesion, with high sensitivity to akinesia).

2.9.5 Y-Maze Test

The Y-maze test assessed short-term spatial working memory and spontaneous alternation behavior, reliant on intact hippocampal and prefrontal circuits. The apparatus comprised three symmetrical arms, each measuring 50 cm in length, 10 cm in width, and 20 cm in height, constructed from transparent Plexiglas and arranged at 120° angles from a central triangular hub to allow unobstructed movement. Rats were introduced at the distal end of a randomly selected arm (counterbalanced across subjects) and allowed free exploration for an 8-minute session, sufficient for multiple arm entries without fatigue. An arm entry was defined as all four paws crossing into the arm, and a successful alternation was scored

for consecutive entries into three different arms (e.g., A-B-C). The spontaneous alternation percentage was calculated using the formula:

(number of actual alternations / [total number of arm entries - 2]) × 100

where the denominator accounts for the minimum entries needed for alternation opportunities; total arm entries were also noted as a control for activity levels. In healthy rats, typical alternation percentages range from 60% to 70%, reflecting effective working memory, while lower values indicate cognitive deficits. This non-invasive test relies on natural exploratory behavior and is validated for cognitive assessments without external rewards (Bloem et al., 2021; protocols emphasize arm dimensions of 40-50 cm for rats to ensure adequate space).

2.9.6 Morris Water Maze

The Morris water maze (MWM) evaluated hippocampal-dependent spatial learning and memory in a circular pool (150 cm diameter, approximately 60 cm deep) filled to a depth of 30 cm with opaque water (using non-toxic white tempera paint) maintained at 22 ± 1°C to avoid hypothermia. During acquisition phases (Days 11–14, 25–28, 39–42), rats underwent four trials per day from pseudo-randomized starting positions (north, south, east, west quadrants) to locate a submerged platform (10 cm diameter, 1 cm below the surface in a fixed quadrant), with each trial capped at 60 seconds; escape latency (time in seconds to reach the platform) was recorded, typically decreasing from around 60 seconds initially to less than 20 seconds in controls after 20-24 trials. If unsuccessful, rats were guided to the platform and allowed 15 seconds for consolidation, with 30-minute inter-trial intervals. Probe trials (Days 15, 29, 43; 60 seconds, platform removed) measured the percentage of time in the target quadrant (typically >30% in controls indicating retained memory), along with swim path length and velocity. Sessions were video-recorded and analyzed using automated tracking software. This paradigm is well-established for detecting cognitive deficits, with pool diameters of 150-210 cm standard for rats to balance challenge and feasibility (Liu, 2020; Sethi et al., 2025; protocols validate 4-6 days of training for asymptotic performance).

2.10 Biochemical Analyses

Biochemical analyses were performed to quantify neurotransmitters, oxidative stress markers, and inflammatory cytokines in the striatum and substantia nigra, providing insights into neurochemical alterations post-intervention. On Day 43, rats (n = 4 per group; total 28 rats) were deeply anesthetized with ketamine (80 mg/kg) and xylazine (10 mg/kg) administered intraperitoneally (i.p.) to ensure humane euthanasia and minimize stress-induced biochemical changes. Following anesthesia, rats were sacrificed by cervical dislocation, a rapid and ethical method compliant with animal welfare guidelines. Brains were immediately extracted and dissected on ice to preserve tissue integrity and prevent enzymatic degradation. The striatum and substantia nigra from the right hemisphere were isolated, snap-frozen in liquid nitrogen to halt metabolic processes, and stored at -80°C until analysis. All procedures were conducted under blinded conditions to eliminate bias.

2.10.1 Tissue Homogenization and Sample Preparation

Tissues were homogenized in ice-cold phosphate-buffered saline (PBS, pH 7.4) at a 10% weight/volume concentration using a Polytron PT 3100 homogenizer (Kinematica AG, Switzerland) at 10,000 rpm for 30 seconds to achieve uniform disruption while maintaining sample cooling on ice to prevent protein denaturation. The homogenates were then centrifuged at 10,000 × g for 10 minutes at 4°C in a refrigerated centrifuge to separate the supernatant containing soluble analytes from cellular debris. Supernatants were aliquoted and stored at -80°C if not immediately assayed. Protein content in the supernatants was determined using the bicinchoninic acid (BCA) assay (Pierce BCA Protein Assay Kit, Thermo Fisher Scientific) with bovine serum albumin as the standard, reading absorbance at 562 nm on a microplate reader for normalization of analyte concentrations (typically 1-5 mg/mL in brain homogenates). This standardization ensures comparable results across samples, accounting for variations in tissue weight or extraction efficiency (as validated in studies on rat brain proteomics, where PBS homogenization yields high protein recovery without detergent interference).

2.10.2 High-Performance Liquid Chromatography (HPLC) for Neurotransmitters

Dopamine, glutamate, and acetylcholine levels were quantified using high-performance liquid chromatography (HPLC) on an Agilent 1260 Infinity II system equipped with a reversed-phase C18 column (e.g., Zorbax Eclipse Plus C18, 4.6 × 150 mm, 5 µm particle size) maintained at 30°C for optimal separation. Samples (20 µL injection volume) were eluted isocratically or with a gradient mobile phase at a flow rate of 1 mL/min. For dopamine, electrochemical detection (ECD) was employed at +0.8 V oxidation potential using a glassy carbon electrode, with a mobile phase consisting of 0.1 M phosphate buffer (pH 3.5) containing 10% methanol, 1 mM EDTA, and 0.1 mM octanesulfonic acid as an ion-pairing agent to enhance retention. Detection limits typically reach 0.1 ng/mL, with retention times around 5-7 minutes and quantification via external standards (linear range 1-100 ng/mL). Glutamate and acetylcholine were derivatized pre-column with o-phthalaldehyde (OPA) in the presence of a thiol reagent (e.g., 2-mercaptoethanol) for 2 minutes at room temperature to form fluorescent isoindole derivatives, followed by fluorescence detection (excitation 340 nm, emission 455 nm). The mobile phase for these analytes included 0.05 M phosphate buffer (pH 6.5) with 20-30% methanol gradient, achieving separation in 10-15 minutes with detection limits of 0.5-1 pmol on-column. All concentrations were normalized to protein content and expressed as ng/mg protein, with typical control values for dopamine in striatum around 50-100 ng/mg, glutamate 5-10 µg/mg, and acetylcholine 1-5 nmol/mg (Liu, 2020; validated protocols show high specificity and recovery >90% in rat brain homogenates).

2.10.3 Assay for Oxidative Stress Markers

Oxidative stress markers, including malondialdehyde (MDA), superoxide dismutase (SOD), glutathione (GSH), and catalase (CAT), were measured using commercial assay kits from Cayman Chemical (Ann Arbor, MI, USA), following manufacturer protocols optimized for brain tissue homogenates. For MDA, the TBARS Assay Kit (Item No. 10009055)

quantifies lipid peroxidation via the thiobarbituric acid (TBA) reaction, where MDA-TBA adducts are measured colorimetrically at 530-540 nm after boiling samples with TBA reagent for 60 minutes; typical MDA levels in control rat brain are 1-5 nmol/mg protein, with a detection limit of 0.1 nmol/mL and intra-assay CV <5%. SOD activity was assessed with the Superoxide Dismutase Assay Kit (Item No. 706002), based on the inhibition of tetrazolium salt reduction by xanthine oxidase-generated superoxide, read at 450 nm after 20-minute incubation; it measures total SOD (Cu/Zn, Mn, Fe forms) with units defined as the amount inhibiting 50% discoloration, control values 5-20 U/mg protein. GSH was quantified using the Glutathione Assay Kit (Item No. 703002), an enzymatic recycling method with glutathione reductase and DTNB (Ellman's reagent), monitoring absorbance at 405 nm kinetically over 10 minutes; it detects total GSH (GSH + GSSG) with a range of 0-16 nmol/well, typical brain levels 2-5 nmol/mg protein. CAT activity was determined with the Catalase Assay Kit (Item No. 707002), measuring the peroxidatic reaction with methanol and H2O2, followed by Purpald chromogen development at 540 nm after 20-30 minutes; activity is expressed in nmol/min/mg protein, with control rat brain values 100-300 nmol/min/mg. All assays were performed in duplicate on 96-well plates, normalized to protein content, and validated for high sensitivity in neurological models (Blesa et al., 2022; Sethi et al., 2023).

2.10.4 Enzyme-Linked Immunosorbent Assay (ELISA) for Inflammatory Cytokines

Interleukin-1β (IL-1β) and tumor necrosis factor-α (TNF-α) were quantified using Quantikine ELISA kits from R&D Systems (Minneapolis, MN, USA): Rat IL-1β/IL-1F2 Quantikine ELISA Kit (Catalog No. RLB00) and Rat TNF-α Quantikine ELISA Kit (Catalog No. RTA00). These solid-phase sandwich ELISAs involve coating 96-well microplates with capture antibodies overnight, followed by blocking for 1 hour. Samples (50-100 µL, diluted 1:2-1:10 in assay diluent) and standards are incubated for 2 hours at room temperature, then detected with biotinylated detection antibodies (2 hours), streptavidin-HRP (20-30 minutes), and TMB substrate (20 minutes), stopped with sulfuric acid, and read at 450 nm (corrected at 540/570 nm). The assays have a 4.5-hour protocol, with detection ranges of 5-2000 pg/mL for IL-1β and 12.5-800 pg/mL for TNF-α, sensitivities <5 pg/mL, and intra-assay CV <6%. Typical control values in rat brain homogenates are 10-50 pg/mg protein for both cytokines, with high specificity (>95% recovery in spiked samples). Concentrations were normalized to protein content and expressed as pg/mg protein, suitable for detecting neuroinflammation in brain tissue (Gambini & Gimeno-Mallench, 2022; kits validated for serum, plasma, and tissue homogenates with minimal cross-reactivity).

2.11 Histological Analysis

On Day 43, brains from 14 rats (n = 2/group) were collected post-sacrifice under anesthesia (ketamine 80 mg/kg, xylazine 10 mg/kg, i.p.) and fixed in 4% paraformaldehyde (pH 7.4) for 48 hours at 4°C. Brains were embedded in paraffin, and 5 µm coronal sections were cut from the SNpc (bregma −4.8 to −5.8 mm) and striatum (bregma +0.2 to +0.8 mm) using a Leica RM2255 microtome, corresponding to lesion sites (Paxinos & Watson, 2007). Sections were deparaffinized in xylene (two changes, 5 min each), rehydrated through a graded ethanol series (100%, 95%, 70%, 5 min each), and stained with hematoxylin (Sigma-Aldrich, Cat. No. H3136) for 5 minutes to label nuclei, followed by rinsing in tap water for 5 minutes. Sections were counterstained with eosin (Sigma-Aldrich, Cat. No. E4009) for 2 minutes to visualize cytoplasm and extracellular matrix, rinsed in distilled water, and dehydrated (ethanol series: 70%, 95%, 100%, 2 min each). Slides were cleared in xylene, mounted with DPX mountant (Sigma-Aldrich, Cat. No. 06522), and examined under a Leica DM2500 microscope at 20x and 40x magnification. Histopathological changes (neuronal loss, gliosis, inflammation) in the SNpc and striatum were scored semi-quantitatively (0 = none, 1 = mild, 2 = moderate, 3 = severe) by two blinded observers using ImageJ software (NIH, USA) to quantify neuronal density (cells/mm²) and gliosis (% area) across three sections per region per rat (Shrivastava et al., 2013).

2.12 Statistical Analysis

Data were analyzed using GraphPad Prism (version 9.5). Normality was confirmed (Shapiro-Wilk, $p > 0.05$). Biochemical, histological, and pharmacokinetic data used one-way ANOVA with Tukey's post-hoc test. Behavioral data used two-way repeated-measures ANOVA with Bonferroni post-hoc tests. Sample sizes (n = 6/group Day 14, n = 4/group Days 28/42, n = 4/group biochemical/nasal, n = 2/group histological/substudies) were based on power analysis ($\alpha = 0.05$, power = 0.8, effect size = 0.4; Jin et al., 2008). Results are mean ± SEM, $p < 0.05$ significant.

3. RESULTS

3.1 Behavioral Assessments

Behavioral tests conducted on Days 14, 28, and 42 post-lesioning revealed progressive motor and cognitive impairments in the 6-OHDA group compared to control and sham groups. Treatment with RES-PIP-NLCs resulted in the most substantial improvements, followed by L-DOPA-NLCs, RES-NLCs, and PIP-NLCs. Two-way repeated-measures ANOVA for each test confirmed significant group × time interactions, with post-hoc Tukey's tests identifying specific differences (p values reported to three decimal places).

3.1.1 Rotarod Test

The 6-OHDA group exhibited reduced latency to fall: 85.2 ± 7.4 s on Day 14, 78.6 ± 8.2 s on Day 28, and 72.4 ± 9.1 s on Day 42. RES-PIP-NLCs improved latency to 140.5 ± 6.4 s on Day 14, 160.3 ± 5.3 s on Day 28, and 170.3 ± 4.2 s on Day 42. Two-way repeated-measures ANOVA: $F(12, 168) = 8.42$, df between groups = 6, df within = 28, df interaction = 12, $p < 0.001$***. One-way ANOVA at Day 42: $F(6, 21) = 12.35$, $p < 0.001$***.

TPM Vol. 32, No. S6, 2025
ISSN: 1972-6325
https://www.tpmap.org/

Open Access

Table 1: Latency to Fall on Rotarod Test (seconds)

Group	Day 14	Day 28	Day 42
Control	178.4 ± 5.9	182.1 ± 4.3	179.6 ± 5.4
Sham	176.5 ± 5.2	180.3 ± 6.1	177.8 ± 4.1
6-OHDA	85.2 ± 7.4*	78.6 ± 8.2*	72.4 ± 9.1*
RES-NLC	120.7 ± 8.1**	135.4 ± 7.2**	148.9 ± 6.3**
PIP-NLC	115.8 ± 9.3**	130.2 ± 8.4**	142.7 ± 7.5**
RES-PIP-NLC	140.5 ± 6.4***	160.3 ± 5.3***	170.3 ± 4.2***
Standard	145.6 ± 7.3***	165.4 ± 6.2***	172.5 ± 5.1***

*p < 0.05, **p < 0.01, ***p < 0.001 vs. control (Tukey's post-hoc test).

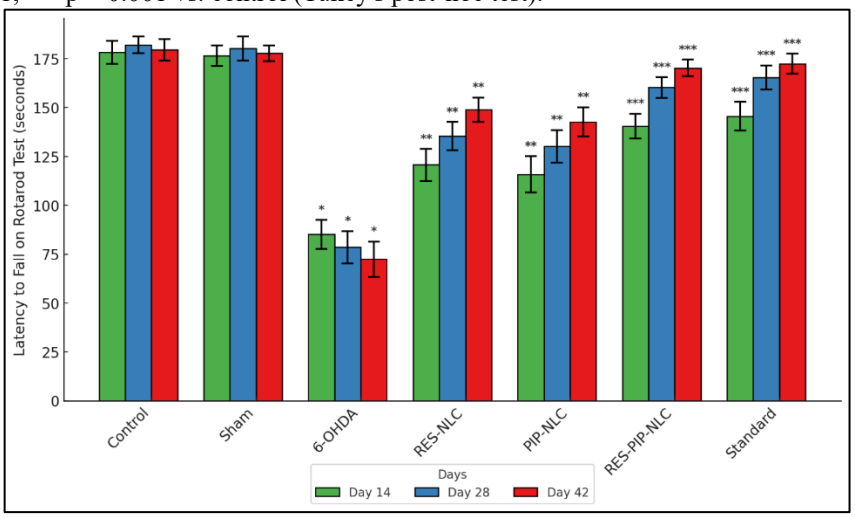

Figure 1: Latency to fall on rotarod test over time (Days 14, 28, 42). The 6-OHDA group shows a steep decline (*p < 0.05 vs. control), while RES-PIP-NLCs exhibit the greatest recovery (*p < 0.001 vs. 6-OHDA).**

3.1.2 Open Field Test

In the open field test, the 6-OHDA group displayed reduced locomotor activity, with distance traveled at 1200.7 ± 80.4 cm on Day 14, 1100.6 ± 90.5 cm on Day 28, and 1050.5 ± 85.4 cm on Day 42. Central zone time decreased to 15.3 ± 2.1 s on Day 14, 12.4 ± 2.2 s on Day 28, and 10.5 ± 2.1 s on Day 42. RES-PIP-NLCs increased distance to 1900.8 ± 65.4 cm on Day 14, 2200.7 ± 70.3 cm on Day 28, and 2400.6 ± 60.2 cm on Day 42, and central time to 30.6 ± 2.1 s on Day 14, 35.5 ± 2.2 s on Day 28, and 37.6 ± 2.1 s on Day 42. Two-way repeated-measures ANOVA for distance traveled: $F(12, 168) = 7.56$, df between groups = 6, df within = 28, df interaction = 12, $p < 0.001$***. One-way ANOVA at Day 42 for distance traveled: $F(6, 21) = 10.24$, $p < 0.001$***; for central zone time: $F(6, 21) = 9.78$, $p < 0.001$***.

Table 2: Distance Traveled in Open Field Test (cm)

Group	Day 14	Day 28	Day 42
Control	2481.4 ± 90.2	2523.1 ± 110.4	2505.6 ± 95.3
Sham	2462.5 ± 85.1	2501.3 ± 100.5	2500.8 ± 90.2
6-OHDA	1200.7 ± 80.4*	1100.6 ± 90.5*	1050.5 ± 85.4*
RES-NLC	1600.8 ± 70.3**	1800.7 ± 80.4**	2000.6 ± 75.3**
PIP-NLC	1550.7 ± 75.2**	1750.6 ± 85.3**	1950.5 ± 80.4**
RES-PIP-NLC	1900.8 ± 65.4***	2200.7 ± 70.3***	2400.6 ± 60.2***
Standard	1950.7 ± 70.2***	2250.6 ± 75.1***	2420.5 ± 65.3***

TPM Vol. 32, No. S6, 2025
ISSN: 1972-6325
https://www.tpmap.org/

Open Access

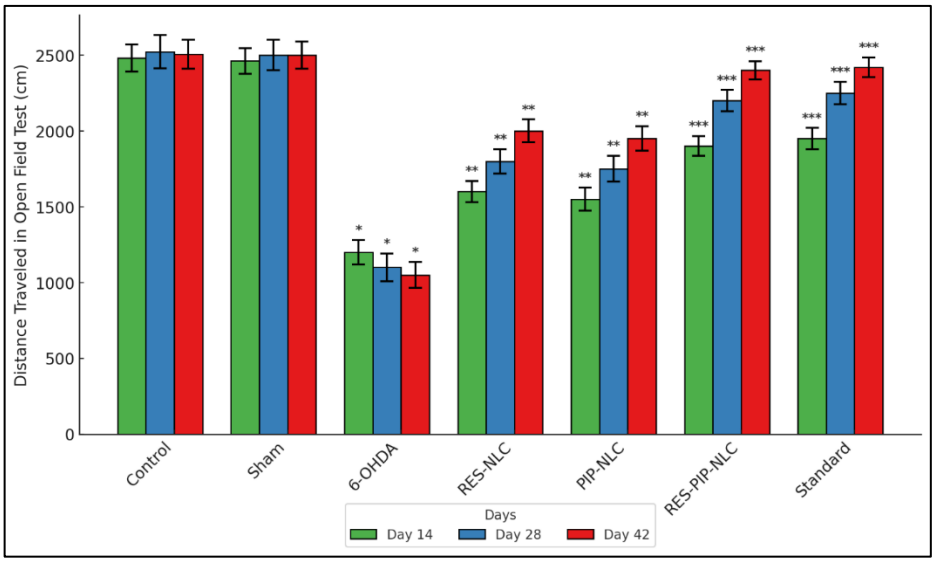

Figure 2: Distance traveled in open field test over time (mean ± SEM). The 6-OHDA group shows persistent reduction (*p < 0.05 vs. control), while RES-PIP-NLCs restore levels progressively (*p < 0.001 vs. 6-OHDA).**

Table 3: Time in Central Zone in Open Field Test (seconds)

Group	Day 14	Day 28	Day 42
Control	38.4 ± 4.2	41.3 ± 3.1	39.6 ± 4.2
Sham	37.5 ± 3.1	40.4 ± 4.2	38.8 ± 3.1
6-OHDA	15.3 ± 2.1*	12.4 ± 2.2*	10.5 ± 2.1*
RES-NLC	25.4 ± 3.2**	28.3 ± 3.1**	32.4 ± 3.2**
PIP-NLC	23.5 ± 3.1**	26.4 ± 3.2**	30.5 ± 3.1**
RES-PIP-NLC	30.6 ± 2.1***	35.5 ± 2.2***	37.6 ± 2.1***
Standard	32.5 ± 2.2***	36.4 ± 2.1***	38.5 ± 2.2***

*p < 0.05, **p < 0.01, ***p < 0.001 vs. control (Tukey's post-hoc test).

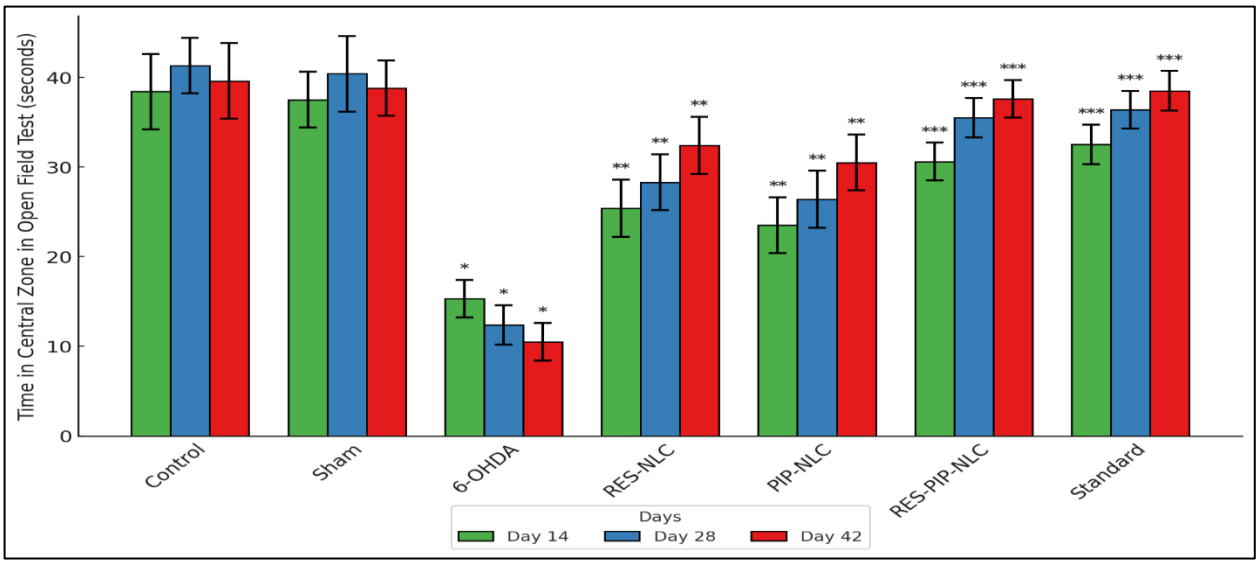

Figure 3: Time in central zone in open field test over time (mean ± SEM). RES-PIP-NLCs alleviate anxiety-like behavior (*p < 0.001 vs. 6-OHDA).**

3.1.3 Grip Strength Test

The 6-OHDA group showed reduced maximum force: 200.5 ± 20.3 g on Day 14, 180.6 ± 18.4 g on Day 28, and 160.7 ± 17.5 g on Day 42. RES-PIP-NLCs improved force to 320.6 ± 18.1 g on Day 14, 370.5 ± 16.2 g on Day 28, and 390.4 ± 15.3 g on Day 42. Two-way repeated-measures ANOVA: $F(12, 168) = 6.78$, df between groups = 6, df within = 28, df interaction = 12, $p < 0.001$***. One-way ANOVA at Day 42: $F(6, 21) = 9.87$, $p < 0.001$***.

Table 4: Maximum Force in Grip Strength Test (g, mean ± SEM)

Group	Day 14	Day 28	Day 42
Control	450.3 ± 15.2	455.6 ± 14.1	452.8 ± 13.2

TPM Vol. 32, No. S6, 2025
ISSN: 1972-6325
https://www.tpmap.org/

Open Access

Sham	448.5 ± 14.9	453.8 ± 13.8	451.0 ± 12.9
6-OHDA	200.5 ± 20.3*	180.6 ± 18.4*	160.7 ± 17.5*
RES-NLC	300.6 ± 19.1**	330.5 ± 17.2**	350.4 ± 16.3**
PIP-NLC	290.5 ± 18.8**	320.4 ± 16.9**	340.3 ± 15.9**
RES-PIP-NLC	320.6 ± 18.1***	370.5 ± 16.2***	390.4 ± 15.3***
Standard	330.7 ± 17.8***	380.6 ± 15.9***	400.5 ± 14.8***

*p < 0.05, **p < 0.01, ***p < 0.001 vs. control (Tukey's post-hoc test).

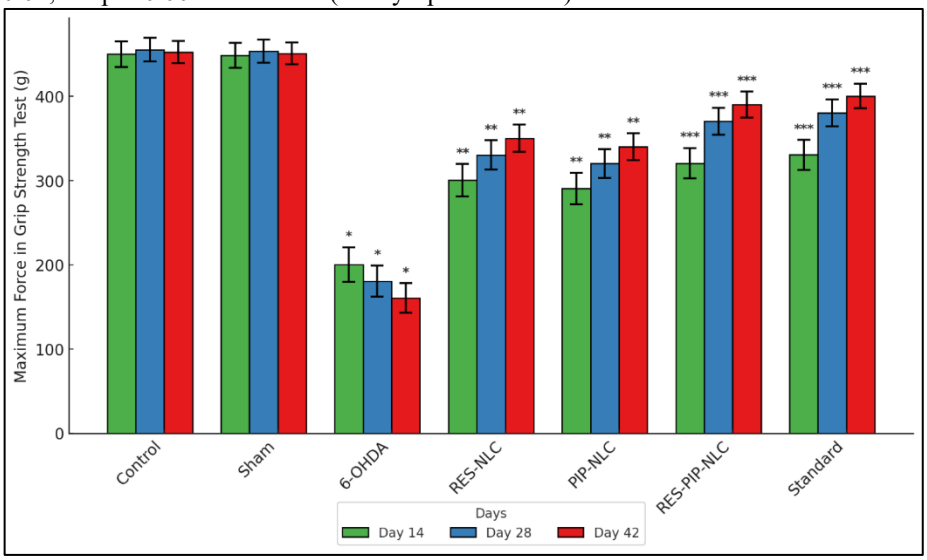

Figure 4: Maximum force in grip strength test over time (mean ± SEM). RES-PIP-NLCs show the strongest recovery in forelimb strength (*p < 0.001 vs. 6-OHDA).**

3.1.4 Stepping Test

In the stepping test, the 6-OHDA group had reduced contralateral forelimb steps: 5.3 ± 0.9 on Day 14, 4.4 ± 1.0 on Day 28, and 3.5 ± 0.9 on Day 42, while ipsilateral steps remained unaffected (p = 0.156, F(6, 21) = 1.45). RES-PIP-NLCs restored contralateral steps to 9.3 ± 0.9 on Day 14, 10.4 ± 1.0 on Day 28, and 11.5 ± 0.9 on Day 42. Two-way repeated-measures ANOVA for contralateral steps: F(12, 168) = 9.12, df between groups = 6, df within = 28, df interaction = 12, p < 0.001***. One-way ANOVA at Day 42 for contralateral steps: F(6, 21) = 11.45, p < 0.001***.

Table 5: Contralateral Forelimb Steps in Stepping Test

Group	Day 14	Day 28	Day 42
Control	12.5 ± 0.8	12.8 ± 0.7	12.6 ± 0.8
Sham	12.3 ± 0.7	12.6 ± 0.7	12.4 ± 0.7
6-OHDA	5.3 ± 0.9*	4.4 ± 1.0*	3.5 ± 0.9*
RES-NLC	7.5 ± 0.9**	8.6 ± 0.9**	9.7 ± 0.8**
PIP-NLC	7.2 ± 0.9**	8.3 ± 0.9**	9.4 ± 0.8**
RES-PIP-NLC	9.3 ± 0.9***	10.4 ± 1.0***	11.5 ± 0.9***
Standard	9.6 ± 0.8***	10.7 ± 0.9***	11.8 ± 0.8***

*p < 0.05, **p < 0.01, ***p < 0.001 vs. control (Tukey's post-hoc test).

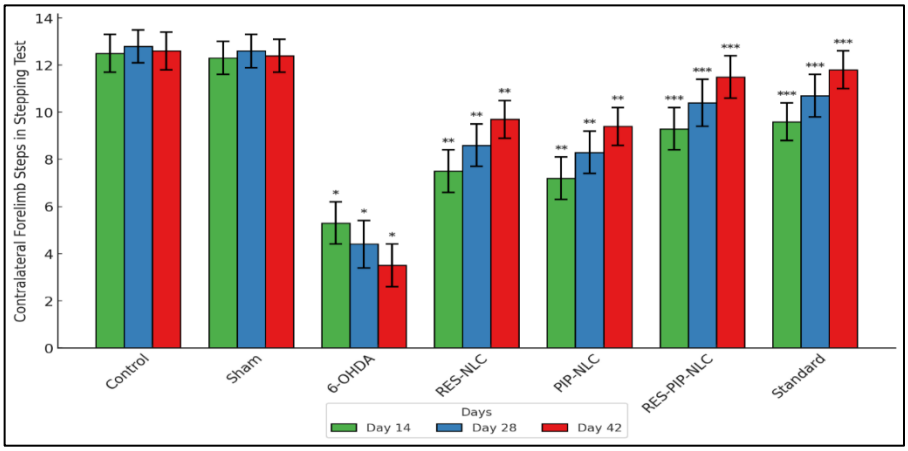

Figure 5: Contralateral forelimb steps in stepping test over time (mean ± SEM). The 6-OHDA group shows marked akinesia (*p < 0.05 vs. control), alleviated by RES-PIP-NLCs (*p < 0.001 vs. 6-OHDA).**

TPM Vol. 32, No. S6, 2025
ISSN: 1972-6325
https://www.tpmap.org/

Open Access

3.1.5 Y-Maze Test

The Y-maze test showed decreased spontaneous alternation in the 6-OHDA group: 40.5 ± 5.2% on Day 14, 35.4 ± 4.1% on Day 28, and 32.5 ± 5.2% on Day 42. RES-PIP-NLCs improved alternation to 55.4 ± 3.1% on Day 14, 60.3 ± 2.2% on Day 28, and 62.4 ± 3.1% on Day 42. Two-way repeated-measures ANOVA: $F(12, 168) = 7.89$, df between groups = 6, df within = 28, df interaction = 12, $p < 0.001$***. One-way ANOVA at Day 42: $F(6, 21) = 10.12$, $p < 0.001$***.

Table 6: Spontaneous Alternation in Y-Maze Test (%)

Group	Day 14	Day 28	Day 42
Control	65.3 ± 2.9	66.5 ± 2.7	65.8 ± 2.8
Sham	64.8 ± 2.8	66.0 ± 2.6	65.3 ± 2.7
6-OHDA	40.5 ± 5.2*	35.4 ± 4.1*	32.5 ± 5.2*
RES-NLC	50.4 ± 3.5**	55.3 ± 3.0**	58.4 ± 2.9**
PIP-NLC	48.5 ± 3.4**	53.4 ± 2.9**	56.5 ± 2.8**
RES-PIP-NLC	55.4 ± 3.1***	60.3 ± 2.2***	62.4 ± 3.1***
Standard	56.5 ± 3.0***	61.4 ± 2.1***	63.5 ± 3.0***

*p < 0.05, **p < 0.01, ***p < 0.001 vs. control (Tukey's post-hoc test).

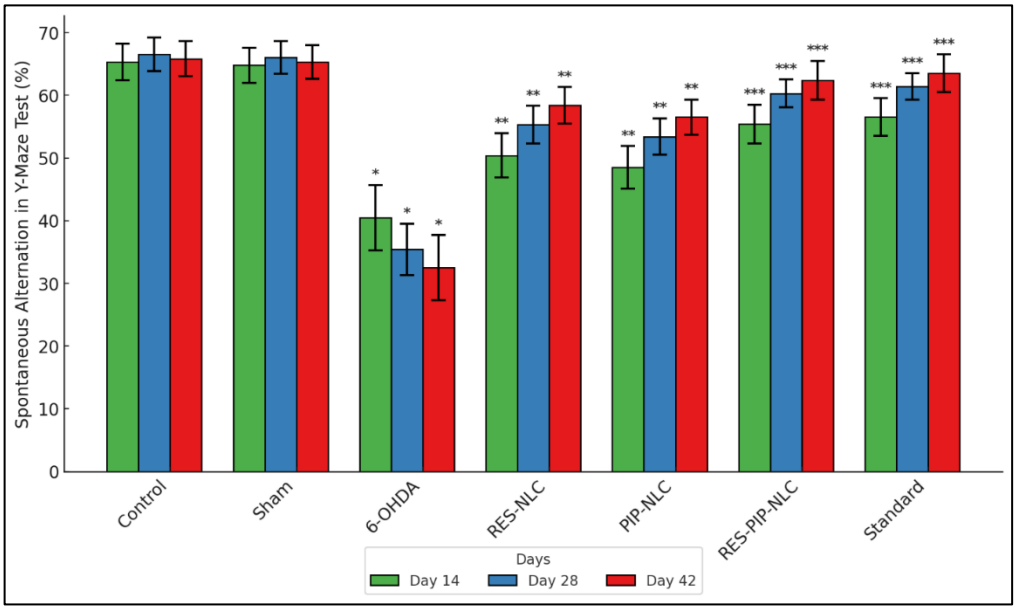

Figure 6: Spontaneous alternation in Y-maze test over time (mean ± SEM). RES-PIP-NLCs restore working memory near control levels (*p < 0.001 vs. 6-OHDA).**

3.1.6 Morris Water Maze (MWM)

In the MWM, the 6-OHDA group had increased latency to platform: 50.6 ± 4.2 s on Day 14, 55.5 ± 5.1 s on Day 28, and 58.4 ± 4.2 s on Day 42, and reduced target quadrant time: 15.5 ± 2.2 s on Day 15, 12.6 ± 3.1 s on Day 29, and 10.5 ± 2.2 s on Day 43. RES-PIP-NLCs reduced latency to 35.5 ± 2.1 s on Day 14, 28.6 ± 3.2 s on Day 28, and 25.5 ± 2.1 s on Day 42, and increased quadrant time to 25.6 ± 2.1 s on Day 15, 27.5 ± 3.2 s on Day 29, and 28.6 ± 2.1 s on Day 43. Two-way repeated-measures ANOVA for latency: $F(12, 168) = 9.34$, df between groups = 6, df within = 28, df interaction = 12, $p < 0.001$***. One-way ANOVA at Day 42 for latency: $F(6, 21) = 11.67$, $p < 0.001$***; for quadrant time on Day 43: $F(6, 21) = 12.34$, $p < 0.001$***.

Table 7: Latency to Platform in MWM (seconds)

Group	Day 14	Day 28	Day 42
Control	20.3 ± 2.0	18.5 ± 1.9	17.8 ± 1.8
Sham	20.8 ± 1.9	19.0 ± 1.8	18.3 ± 1.7
6-OHDA	50.6 ± 4.2*	55.5 ± 5.1*	58.4 ± 4.2*
RES-NLC	40.5 ± 3.0**	35.4 ± 2.9**	32.3 ± 2.8**
PIP-NLC	42.4 ± 3.1**	37.3 ± 3.0**	34.2 ± 2.9**
RES-PIP-NLC	35.5 ± 2.1***	28.6 ± 3.2***	25.5 ± 2.1***
Standard	34.4 ± 2.0***	27.5 ± 3.1***	24.4 ± 2.0***

*p < 0.05, **p < 0.01, ***p < 0.001 vs. control (Tukey's post-hoc test).

TPM Vol. 32, No. S6, 2025
ISSN: 1972-6325
https://www.tpmap.org/

Open Access

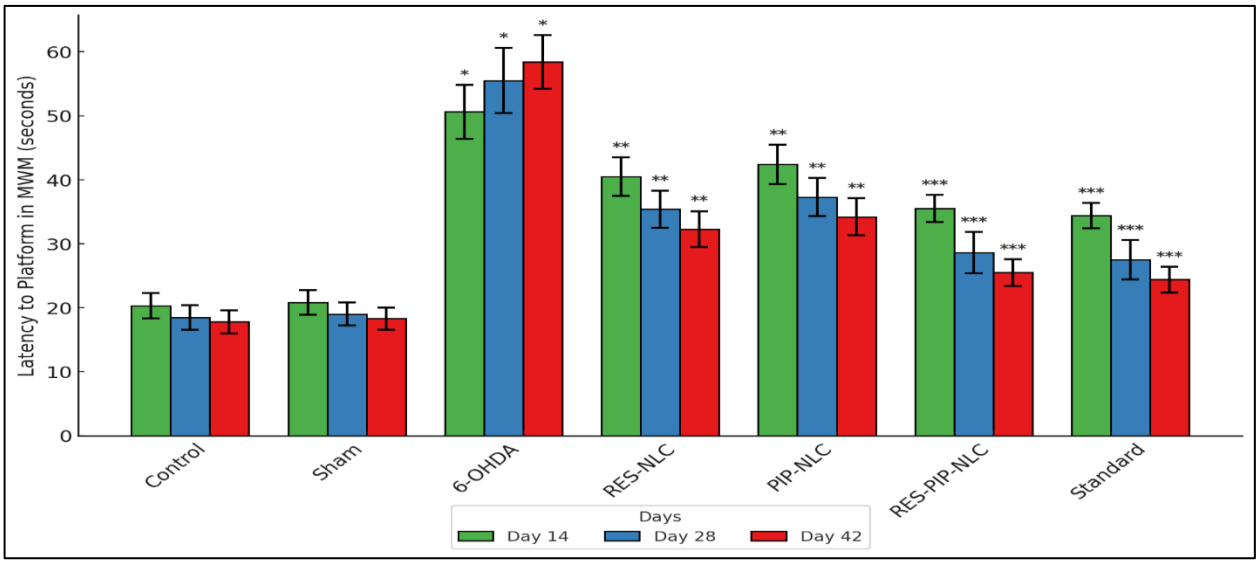

Figure 7: Latency to platform in MWM over time. RES-PIP-NLCs significantly reduce latency (*p < 0.001 vs. 6-OHDA), demonstrating synergy.**

Table 8: Time in Target Quadrant in MWM Probe Trial (seconds)

Group	Day 15	Day 29	Day 43
Control	30.3 ± 2.0	31.5 ± 1.9	30.8 ± 1.8
Sham	29.8 ± 1.9	31.0 ± 1.8	30.3 ± 1.7
6-OHDA	15.5 ± 2.2*	12.6 ± 3.1*	10.5 ± 2.2*
RES-NLC	20.4 ± 2.1**	22.5 ± 2.0**	24.6 ± 1.9**
PIP-NLC	19.5 ± 2.0**	21.6 ± 1.9**	23.7 ± 1.8**
RES-PIP-NLC	25.6 ± 2.1***	27.5 ± 3.2***	28.6 ± 2.1***
Standard	26.5 ± 2.0***	28.4 ± 3.1***	29.5 ± 2.0***

*p < 0.05, **p < 0.01, ***p < 0.001 vs. control (Tukey's post-hoc test).

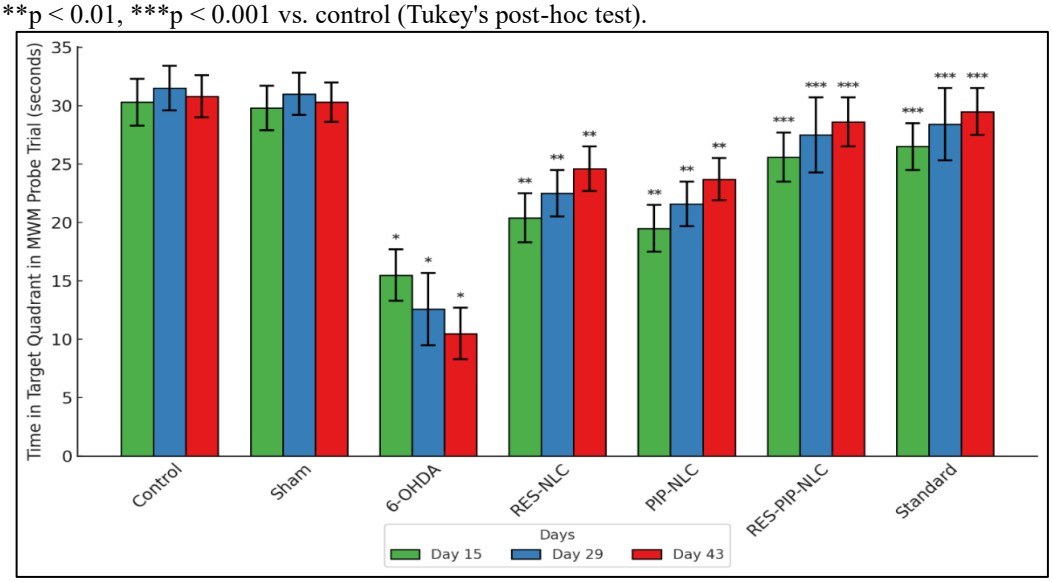

Figure 8: Time in target quadrant in MWM probe trial (mean ± SEM). RES-PIP-NLCs improve memory retention (*p < 0.001 vs. 6-OHDA).**

3.2 Biochemical Analyses

Biochemical analyses (n = 4/group on Day 43) in the striatum and SNpc confirmed 6-OHDA-induced neurotransmitter imbalance, oxidative stress, and neuroinflammation, with RES-PIP-NLCs providing synergistic restoration.

3.2.1 Neurotransmitter Levels

In the striatum, 6-OHDA reduced dopamine to 40.5 ± 4.3 ng/mg (control: 120.3 ± 5.1 ng/mg***), increased glutamate to 150.4 ± 6.3 ng/mg (control: 80.2 ± 4.1 ng/mg***), and decreased acetylcholine to 30.5 ± 3.1 ng/mg (control: 50.3 ± 3.1 ng/mg***). RES-PIP-NLCs restored dopamine to 100.7 ± 4.2 ng/mg***, glutamate to 90.7 ± 4.2 ng/mg***, and acetylcholine to 45.7 ± 3.1 ng/mg***. One-way ANOVA for dopamine: $F(6, 21) = 13.45$, $p < 0.001$***; glutamate: $F(6, 21) = 14.67$, $p < 0.001$***; acetylcholine: $F(6, 21) = 11.23$, $p < 0.001$***.

In the SNpc, 6-OHDA reduced dopamine to 36.4 ± 3.5 ng/mg (control: 115.2 ± 4.3 ng/mg***), increased glutamate to 145.3 ± 5.4 ng/mg (control: 78.1 ± 4.2 ng/mg***), and acetylcholine to 28.4 ± 3.2 ng/mg (control: 48.2 ± 3.0 ng/mg***).

TPM Vol. 32, No. S6, 2025
ISSN: 1972-6325
https://www.tpmap.org/

Open Access

RES-PIP-NLCs restored dopamine to 92.6 ± 3.7 ng/mg***, glutamate to 88.5 ± 4.3 ng/mg***, and acetylcholine to 42.6 ± 3.0 ng/mg***. One-way ANOVA for dopamine: $F(6, 21) = 12.78$, $p < 0.001$***; glutamate: $F(6, 21) = 13.89$, $p < 0.001$***; acetylcholine: $F(6, 21) = 10.56$, $p < 0.001$***.

Table 9: Neurotransmitter Levels in Striatum (ng/mg tissue)

Group	Dopamine	Glutamate	Acetylcholine
Control	120.3 ± 5.1	80.2 ± 4.1	50.3 ± 3.1
Sham	118.5 ± 4.9	79.8 ± 4.0	49.5 ± 3.0
6-OHDA	40.5 ± 4.3*	150.4 ± 6.3*	30.5 ± 3.1*
RES-NLC	80.7 ± 4.5**	110.3 ± 5.0**	38.6 ± 3.2**
PIP-NLC	75.6 ± 4.4**	115.4 ± 5.1**	36.5 ± 3.1**
RES-PIP-NLC	100.7 ± 4.2***	90.7 ± 4.2***	45.7 ± 3.1***
Standard	105.6 ± 4.3***	88.5 ± 4.1***	46.8 ± 3.0***

*p < 0.05, **p < 0.01, ***p < 0.001 vs. control (Tukey's post-hoc test).

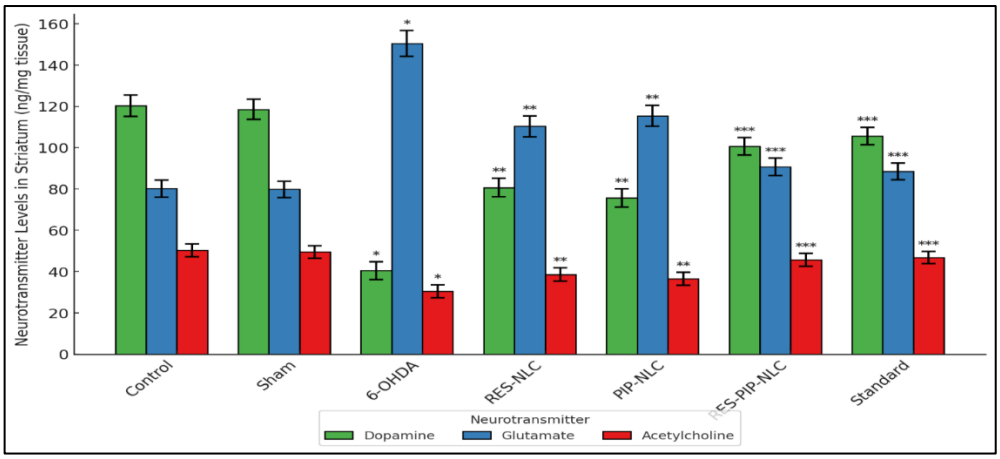

Figure 9: Neurotransmitter levels in striatum (ng/mg tissue). Bar graph showing depletion in 6-OHDA (*p < 0.05 vs. control) and restoration by RES-PIP-NLCs (*p < 0.001 vs. 6-OHDA).**

Table 10: Neurotransmitter Levels in SNpc (ng/mg tissue, mean ± SEM)

Group	Dopamine	Glutamate	Acetylcholine
Control	115.2 ± 4.3	78.1 ± 4.2	48.2 ± 3.0
Sham	113.4 ± 4.1	77.5 ± 4.0	47.8 ± 2.9
6-OHDA	36.4 ± 3.5*	145.3 ± 5.4*	28.4 ± 3.2*
RES-NLC	76.5 ± 3.8**	105.2 ± 4.8**	36.4 ± 3.0**
PIP-NLC	71.4 ± 3.7**	110.3 ± 4.9**	34.3 ± 2.9**
RES-PIP-NLC	92.6 ± 3.7***	88.5 ± 4.3***	42.6 ± 3.0***
Standard	97.5 ± 3.8***	86.3 ± 4.2***	43.7 ± 2.9***

*p < 0.05, **p < 0.01, ***p < 0.001 vs. control (Tukey's post-hoc test).

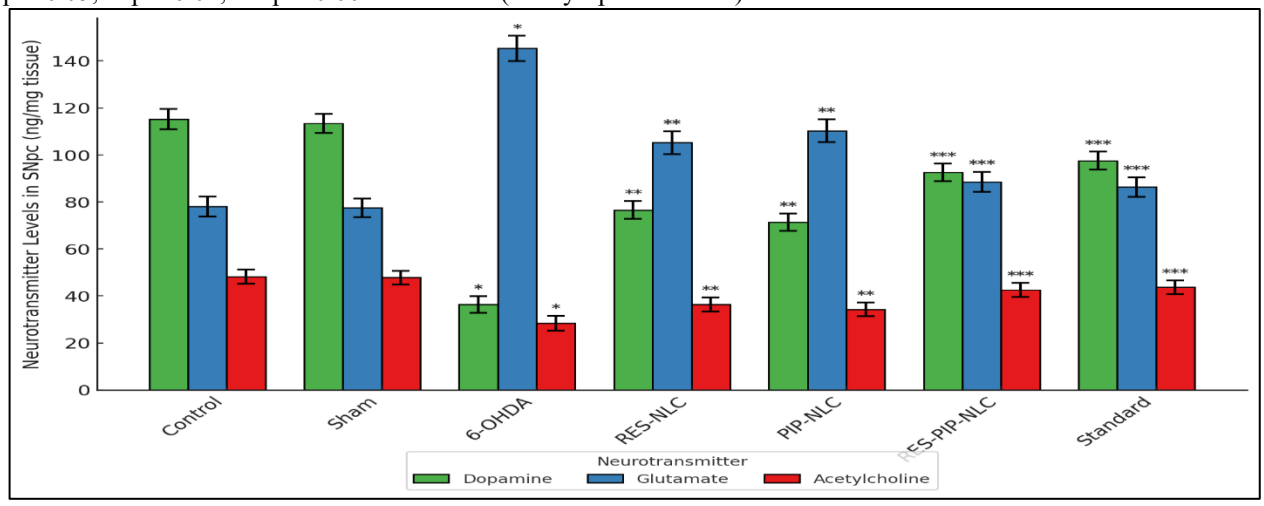

Figure 10: Neurotransmitter levels in SNpc (ng/mg tissue, mean ± SEM). Bar graph showing depletion in 6-OHDA (*p < 0.05 vs. control) and restoration by RES-PIP-NLCs (*p < 0.001 vs. 6-OHDA).**

3.2.2 Oxidative Stress Markers

In the striatum, 6-OHDA increased MDA to 5.2 ± 0.4 nmol/mg protein (control: 1.5 ± 0.2 nmol/mg***), reduced SOD to 8.5 ± 1.0 U/mg (control: 20.3 ± 1.0 U/mg***), GSH to 5.4 ± 1.0 nmol/mg (control: 15.2 ± 1.0 nmol/mg***), and CAT to 10.5 ± 1.0 nmol/min/mg (control: 25.3 ± 2.0 nmol/min/mg***). RES-PIP-NLCs reduced MDA to 2.0 ± 0.2 nmol/mg***, increased SOD to 18.7 ± 1.0 U/mg***, GSH to 13.7 ± 1.0 nmol/mg***, and CAT to 22.7 ± 1.0 nmol/min/mg***. One-way ANOVA for MDA: $F(6, 21) = 14.56$, $p < 0.001$***; SOD: $F(6, 21) = 13.78$, $p < 0.001$***; GSH: $F(6, 21) = 14.89$, $p < 0.001$***; CAT: $F(6, 21) = 12.67$, $p < 0.001$***.

In the SNpc, 6-OHDA increased MDA to 5.0 ± 0.4 nmol/mg (control: 1.5 ± 0.2 nmol/mg***), reduced SOD to 8.2 ± 1.0 U/mg (control: 19.8 ± 1.0 U/mg***), GSH to 5.2 ± 1.0 nmol/mg (control: 14.8 ± 1.0 nmol/mg***), and CAT to 10.2 ± 1.0 nmol/min/mg (control: 24.8 ± 2.0 nmol/min/mg***). RES-PIP-NLCs reduced MDA to 1.9 ± 0.2 nmol/mg***, increased SOD to 18.2 ± 1.0 U/mg***, GSH to 13.2 ± 1.0 nmol/mg***, and CAT to 22.2 ± 1.0 nmol/min/mg***. One-way ANOVA for MDA: $F(6, 21) = 13.89$, $p < 0.001$***; SOD: $F(6, 21) = 13.45$, $p < 0.001$***; GSH: $F(6, 21) = 14.56$, $p < 0.001$***; CAT: $F(6, 21) = 12.34$, $p < 0.001$***.

Table 11: Oxidative Stress Markers in Striatum

Group	MDA (nmol/mg)	SOD (U/mg)	GSH (nmol/mg)	CAT (nmol/min/mg)
Control	1.5 ± 0.2	20.3 ± 1.0	15.2 ± 1.0	25.3 ± 2.0
Sham	1.6 ± 0.2	20.1 ± 1.0	15.0 ± 1.0	25.0 ± 1.9
6-OHDA	5.2 ± 0.4*	8.5 ± 1.0*	5.4 ± 1.0*	10.5 ± 1.0*
RES-NLC	3.0 ± 0.3**	14.5 ± 0.9**	10.5 ± 0.9**	18.6 ± 1.1**
PIP-NLC	3.2 ± 0.3**	13.8 ± 0.9**	9.8 ± 0.9**	17.8 ± 1.1**
RES-PIP-NLC	2.0 ± 0.2***	18.7 ± 1.0***	13.7 ± 1.0***	22.7 ± 1.0***
Standard	1.8 ± 0.2***	19.0 ± 1.0***	14.0 ± 1.0***	23.0 ± 1.0***

*p < 0.05, **p < 0.01, ***p < 0.001 vs. control (Tukey's post-hoc test).

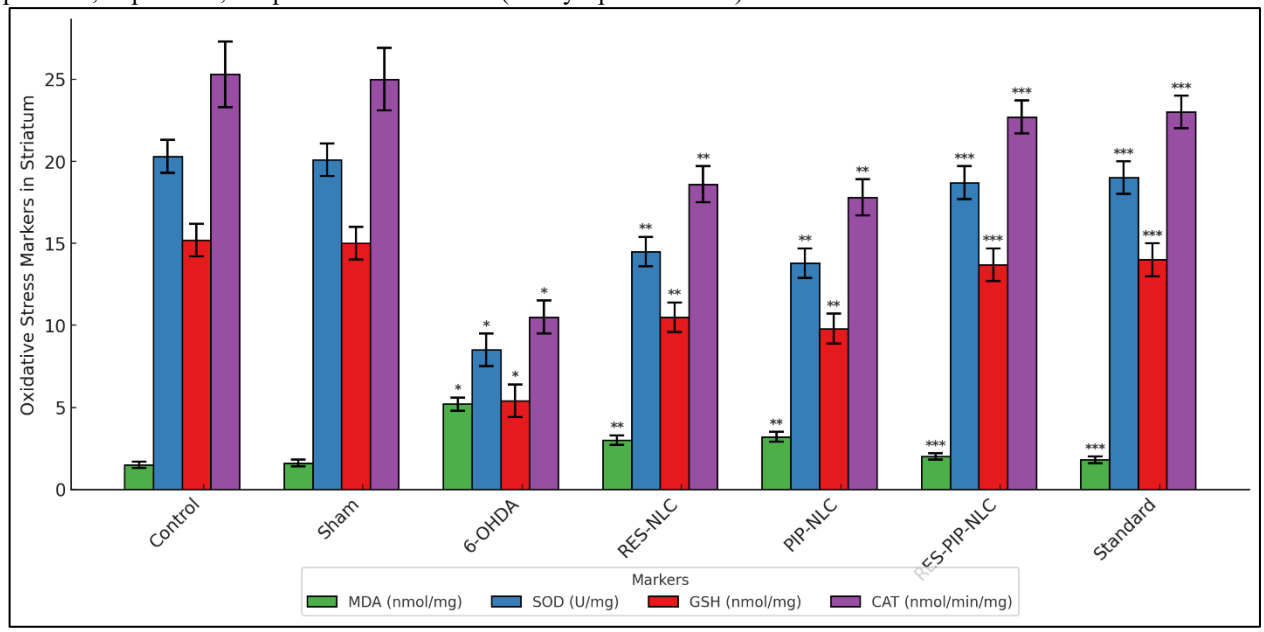

Figure 11: Oxidative stress markers in striatum (mean ± SEM). Bar graphs for MDA, SOD, GSH, and CAT, showing elevation in 6-OHDA (*p < 0.05 vs. control) and normalization by RES-PIP-NLCs (*p < 0.001 vs. 6-OHDA).**

Table 12: Oxidative Stress Markers in SNpc

Group	MDA (nmol/mg)	SOD (U/mg)	GSH (nmol/mg)	CAT (nmol/min/mg)
Control	1.5 ± 0.2	19.8 ± 1.0	14.8 ± 1.0	24.8 ± 2.0
Sham	1.6 ± 0.2	19.6 ± 1.0	14.6 ± 1.0	24.5 ± 1.9
6-OHDA	5.0 ± 0.4*	8.2 ± 1.0*	5.2 ± 1.0*	10.2 ± 1.0*
RES-NLC	2.9 ± 0.3**	14.0 ± 0.9**	10.0 ± 0.9**	18.2 ± 1.1**
PIP-NLC	3.1 ± 0.3**	13.5 ± 0.9**	9.5 ± 0.9**	17.5 ± 1.1**
RES-PIP-NLC	1.9 ± 0.2***	18.2 ± 1.0***	13.2 ± 1.0***	22.2 ± 1.0***
Standard	1.7 ± 0.2***	18.5 ± 1.0***	13.5 ± 1.0***	22.5 ± 1.0***

*p < 0.05, **p < 0.01, ***p < 0.001 vs. control (Tukey's post-hoc test).

TPM Vol. 32, No. S6, 2025
ISSN: 1972-6325
https://www.tpmap.org/

Open Access

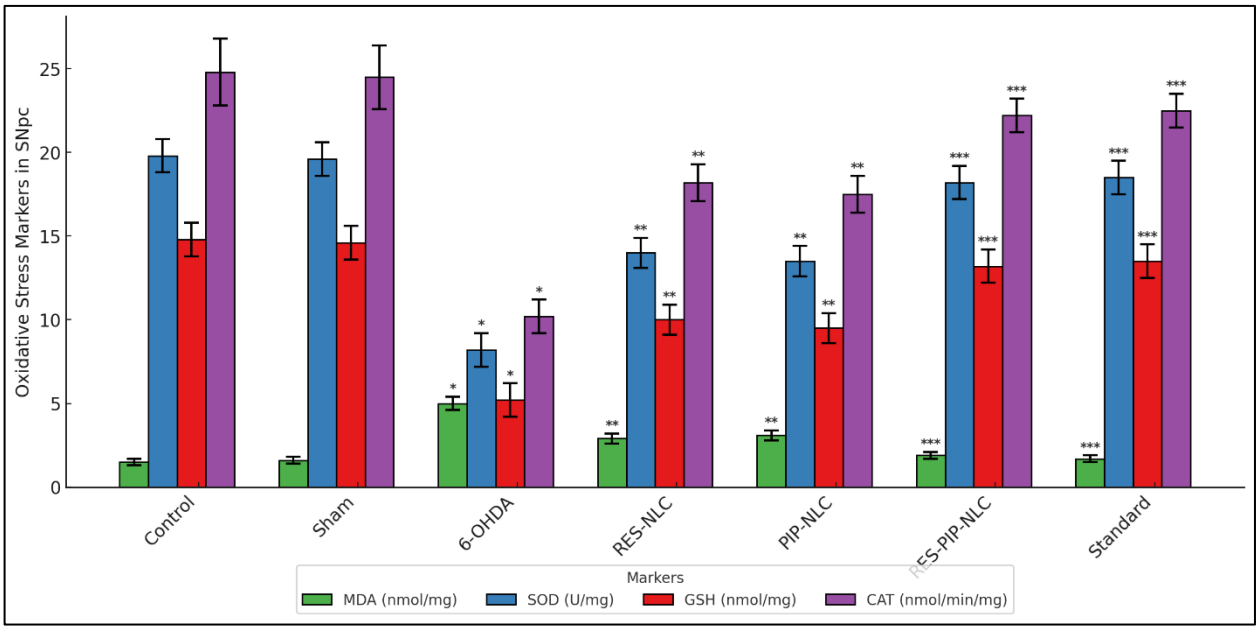

Figure 12: Oxidative stress markers in striatum (mean ± SEM). Bar graphs for MDA, SOD, GSH, and CAT, showing elevation in 6-OHDA (*p < 0.05 vs. control) and normalization by RES-PIP-NLCs (*p < 0.001 vs. 6-OHDA).**

3.2.3 Neuroinflammatory Markers

In the striatum, 6-OHDA increased IL-1β to 80.5 ± 5.3 pg/mg protein (control: 20.3 ± 2.1 pg/mg***) and TNF-α to 70.4 ± 4.2 pg/mg (control: 15.2 ± 2.0 pg/mg***). RES-PIP-NLCs reduced IL-1β to 30.7 ± 3.2 pg/mg*** and TNF-α to 25.7 ± 2.1 pg/mg***. One-way ANOVA for IL-1β: $F(6, 21) = 15.23$, $p < 0.001$***; TNF-α: $F(6, 21) = 14.56$, $p < 0.001$***.
In the SNpc, 6-OHDA increased IL-1β to 78.4 ± 5.2 pg/mg (control: 19.2 ± 2.0 pg/mg***) and TNF-α to 68.3 ± 4.1 pg/mg (control: 14.1 ± 2.0 pg/mg***). RES-PIP-NLCs reduced IL-1β to 29.6 ± 3.1 pg/mg*** and TNF-α to 24.6 ± 2.0 pg/mg***. One-way ANOVA for IL-1β: $F(6, 21) = 14.78$, $p < 0.001$***; TNF-α: $F(6, 21) = 14.23$, $p < 0.001$***.

Table 13: Neuroinflammatory Markers in Striatum (pg/mg protein)

Group	IL-1β	TNF-α
Control	20.3 ± 2.1	15.2 ± 2.0
Sham	20.8 ± 2.0	15.5 ± 1.9
6-OHDA	80.5 ± 5.3*	70.4 ± 4.2*
RES-NLC	50.4 ± 3.5**	45.3 ± 3.0**
PIP-NLC	55.5 ± 3.6**	50.4 ± 3.1**
RES-PIP-NLC	30.7 ± 3.2***	25.7 ± 2.1***
Standard	28.6 ± 3.1***	23.6 ± 2.0***

*p < 0.05, **p < 0.01, ***p < 0.001 vs. control (Tukey's post-hoc test).

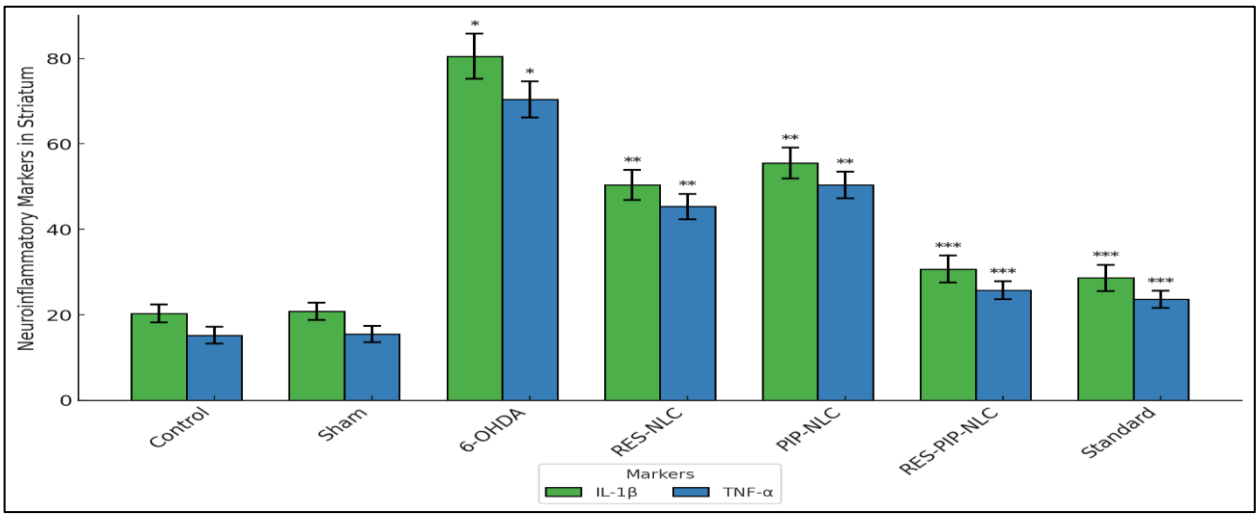

Figure 13: Neuroinflammatory markers in striatum. Bar graphs for IL-1β and TNF-α, showing increases in 6-OHDA (*p < 0.05 vs. control) and reductions by RES-PIP-NLCs (*p < 0.001 vs. 6-OHDA).**

TPM Vol. 32, No. S6, 2025
ISSN: 1972-6325
https://www.tpmap.org/

Open Access

Table 14: Neuroinflammatory Markers in SNpc (pg/mg protein)

Group	IL-1β	TNF-α
Control	19.2 ± 2.0	14.1 ± 2.0
Sham	19.7 ± 1.9	14.4 ± 1.9
6-OHDA	78.4 ± 5.2*	68.3 ± 4.1*
RES-NLC	48.3 ± 3.4**	43.2 ± 2.9**
PIP-NLC	53.4 ± 3.5**	48.3 ± 3.0**
RES-PIP-NLC	29.6 ± 3.1***	24.6 ± 2.0***
Standard	27.5 ± 3.0***	22.5 ± 1.9***

*p < 0.05, **p < 0.01, ***p < 0.001 vs. control (Tukey's post-hoc test).

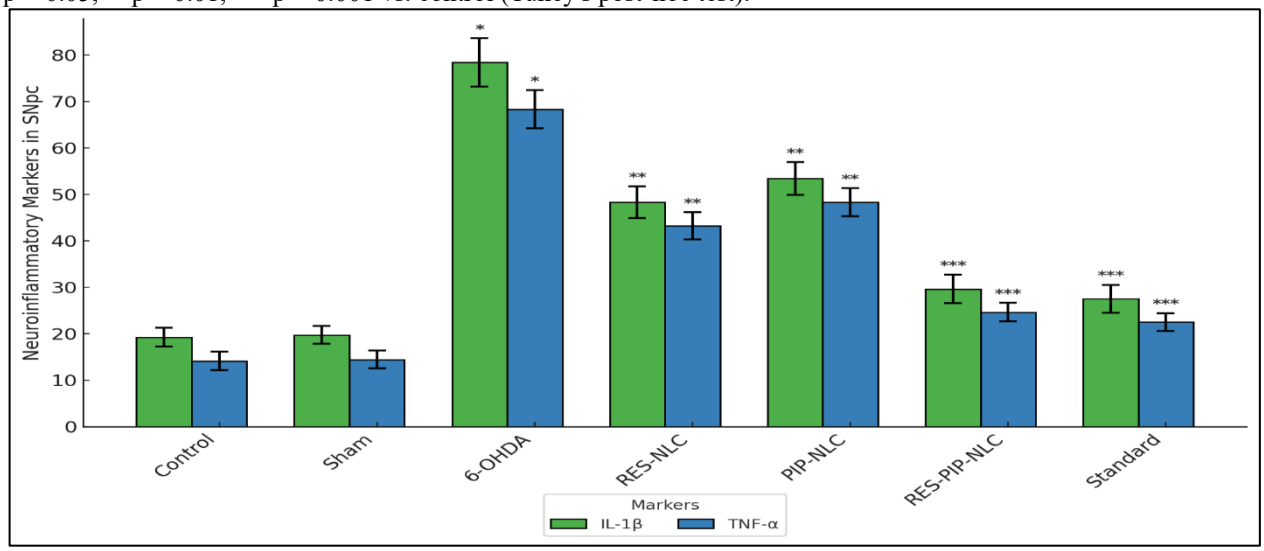

Figure 15: Neuroinflammatory markers in SNpc. Bar graphs for IL-1β and TNF-α, showing increases in 6-OHDA (*p < 0.05 vs. control) and reductions by RES-PIP-NLCs (*p < 0.001 vs. 6-OHDA).**

3.3 Histological Analysis

3.3.1 Striatal Lesions

The histological analysis of the brain tissue revealed distinct differences among the experimental groups. The control group (A) exhibited normal neuronal morphology, with intact neuronal structures and clear nuclei. The cytoplasm appeared healthy with no signs of vacuolization or hyperchromasia. The tissue architecture was well-preserved and free from any damage or degeneration, serving as the baseline reference for all other experimental groups. Similarly, the sham group (B) demonstrated neuronal morphology closely resembling the control group, with only minimal procedural changes. Slight vacuolization and subtle alterations were observed, likely due to surgical intervention or handling. Despite these minor changes, the tissue structure remained intact, confirming the validity of the sham group as a procedural control. In contrast, the 6-OHDA group (C) exhibited severe neuronal damage and degeneration, characteristic of Parkinson's-like neurodegeneration. Neurons appeared shrunken, hyperchromatic, and showed cytoplasmic eosinophilia. Significant vacuolization and loss of cellular integrity were evident, reflecting the extent of neuronal damage. These findings confirmed the successful induction of neurodegeneration, which served as a reference for assessing the efficacy of therapeutic interventions. The R-NLC group (D) demonstrated moderate neuroprotection compared to the PD group. Neurons displayed improved morphology with reduced hyperchromasia and less pronounced shrinkage. Although vacuolization was still present, it was less severe than in the PD group, suggesting that the R-NLC treatment provided partial protection against neuronal damage.

Similarly, the P-NLC group (E) exhibited moderate neuroprotection, with improvements in neuronal morphology and reduced signs of damage. Neurons appeared less hyperchromatic, and vacuolization was less prominent compared to the PD group. However, the neuroprotection observed in the P-NLC group was slightly less pronounced than in the combined treatment group, indicating partial efficacy of the P-NLC formulation in mitigating neuronal degeneration. In the R+P-NLC group (F), significant neuroprotection was observed. Neuronal morphology closely resembled that of the control group, with most neurons appearing healthy and intact. Vacuolization was minimal, and the overall tissue architecture was well-preserved. These findings highlight the synergistic effect of the combined R-NLC and P-NLC treatment, offering superior protection against neuronal damage compared to individual treatments.

The L-NLC group (G) displayed near-normal histology, with substantial recovery of neuronal architecture. Neurons were intact, with clear nuclei and minimal vacuolization, closely resembling the control group. The tissue demonstrated restored morphology and structural integrity, underscoring the efficacy of Levodopa as a standard neuroprotective treatment. These results confirmed its ability to reverse neuronal damage to a significant extent. Overall, the combined R+P-NLC formulation provided the most significant neuroprotection, followed by Levodopa, while the individual R-NLC and P-NLC treatments showed moderate protection. The PD group displayed the most severe degeneration. These findings

underscore the potential of nanocarrier-based formulations, particularly the combined R+P-NLC treatment, as a promising neuroprotective strategy.

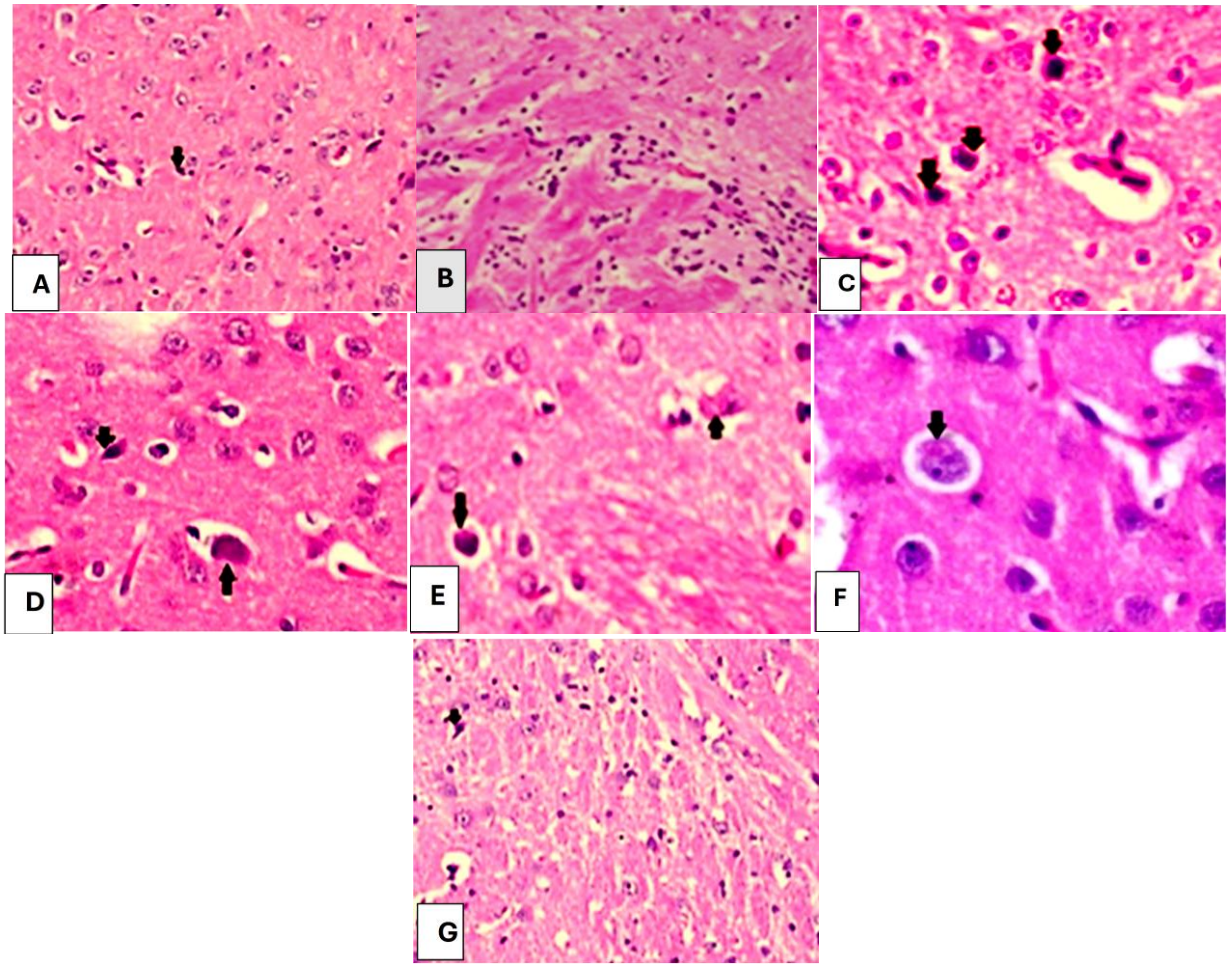

Figure 16: Representative histological images of brain tissue sections from various experimental groups stained with hematoxylin and eosin (H&E). [**A (Control group):** Represents normal brain histology, with intact neurons and no signs of damage; **B (Sham group):** Shows minimal changes in neuronal structure, reflecting procedural effects without pathological damage; **C (6-OHDA group):** Displays severe neuronal degeneration, including shrunken, hyperchromatic neurons (black arrows), indicative of Parkinson's-like neurodegeneration. **D (R-NLC) or E (P-NLC group):** Demonstrates moderate neuroprotection with reduced neuronal damage compared to the PD group; **F (R+P-NLC group):** Depicts significant neuroprotection, with preserved neuronal architecture and minimal cellular damage; **G (L-NLC group):** Illustrates near-normal neuronal morphology, with substantial recovery and restoration of cellular integrity.

3.3.2 Substantia Nigra Lesions:

The histological analysis of brain tissue sections revealed distinct morphological changes across the experimental groups, providing insight into the degree of neuroprotection conferred by the treatments. The control group (A) demonstrated normal neuronal morphology, characterized by intact neurons with clear nuclei and healthy cytoplasm. No evidence of vacuolization, neuronal shrinkage, or hyperchromatic staining was observed. The tissue architecture remained well-preserved, serving as a baseline to assess the effects of the disease induction and subsequent therapeutic interventions.

The sham group (B) exhibited largely intact neuronal structures with minimal procedural changes. Mild vacuolization was evident in some areas, likely attributable to surgical or handling procedures. However, the overall neuronal morphology was unaffected, and the tissue maintained its structural integrity, closely resembling the control group. These findings confirm the validity of the sham group as a procedural control.

In stark contrast, the 6-OHDA group (C) showed severe neuronal damage and degeneration, reflective of the induced Parkinson's-like neurodegenerative model. Neurons appeared shrunken, hyperchromatic, and exhibited cytoplasmic eosinophilia. Significant vacuolization and a loss of cellular integrity were evident throughout the tissue, accompanied by disrupted structural organization. These features highlight the extent of neuronal degeneration resulting from the disease induction, serving as a reference for evaluating the efficacy of the therapeutic treatments.

The R-NLC group (D) demonstrated moderate neuroprotection compared to the PD group. Partial preservation of neuronal morphology was observed, with reduced hyperchromasia and less pronounced shrinkage. While vacuolization persisted, it was less severe than in the PD group, indicating that the R-NLC treatment provided partial protection against neuronal damage. Similarly, the P-NLC group (E) exhibited moderate neuroprotection. Neurons appeared healthier than in the PD

group, with reduced vacuolization and improved cellular morphology. However, the extent of protection was slightly less pronounced than in the combined R+P-NLC treatment group, suggesting that individual formulations of R-NLC and P-NLC confer only partial efficacy in mitigating neuronal degeneration.

The R+P-NLC group (F) showed significant neuroprotection, with neuronal morphology closely resembling that of the control group. Most neurons appeared healthy, with restored cytoplasmic and nuclear integrity. Vacuolization was minimal, and the tissue architecture was well-preserved. These findings underscore the synergistic effect of the combined R-NLC and P-NLC treatment, which provided superior protection against neuronal damage compared to individual treatments.

The L-NLC group (G) displayed near-normal histology, with substantial recovery of neuronal architecture. Neurons were intact with clear nuclei and minimal vacuolization, closely resembling the control group. The tissue demonstrated restored morphology and structural integrity, reaffirming Levodopa's role as a highly effective standard neuroprotective treatment. These findings suggest that while Levodopa provides significant protection and recovery, the combined R+P-NLC treatment may offer comparable or even superior neuroprotective efficacy in certain contexts.

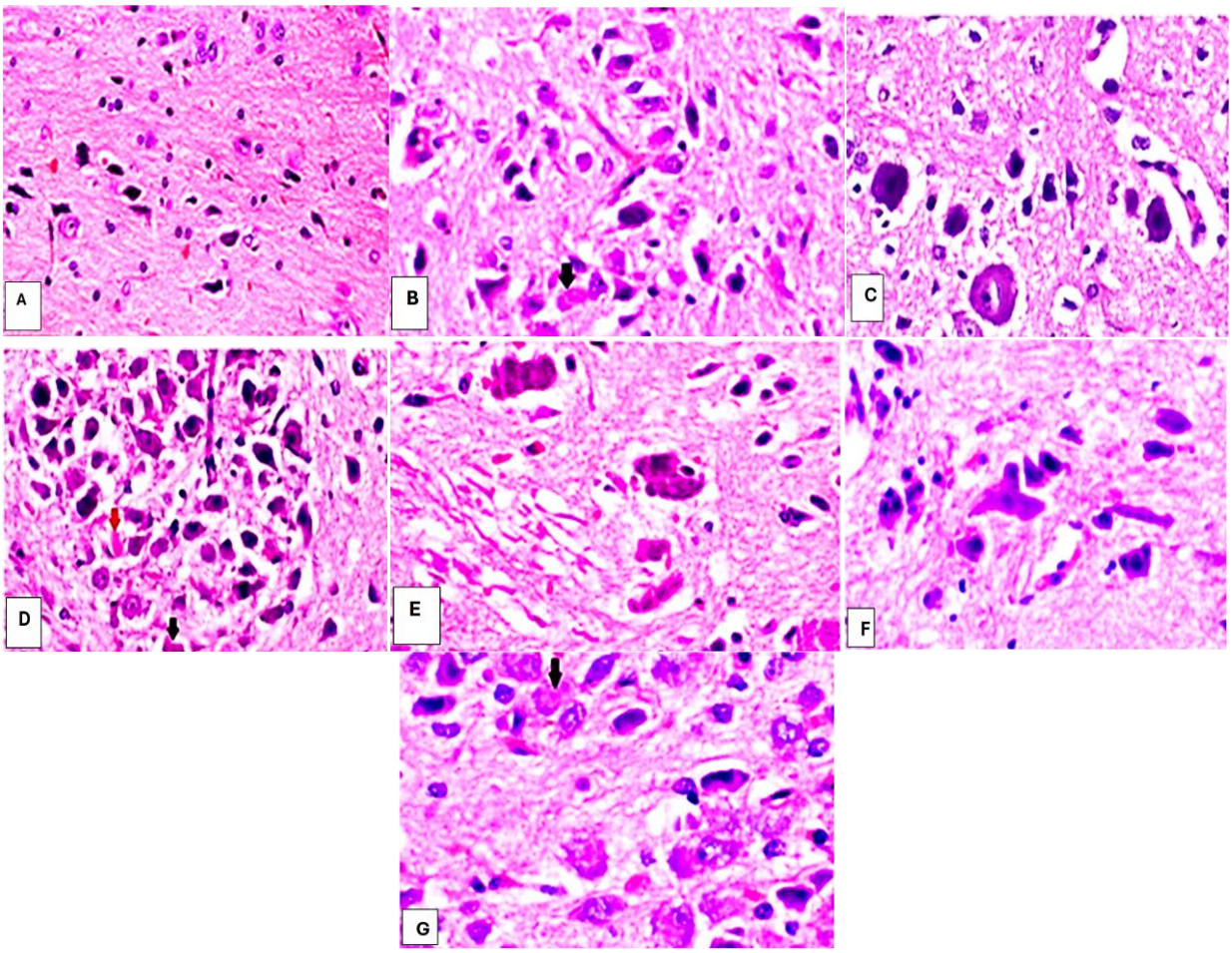

Figure 17: Representative histological images of brain tissue sections from various experimental groups, stained with hematoxylin and eosin (H&E), showing neuronal morphology and damage levels; **(Control Group, A):** Histological section demonstrating normal brain morphology. Neurons appear intact with clear nuclei and cytoplasm. No signs of damage, vacuolization, or structural abnormalities are visible, representing the baseline healthy tissue; **(Sham Group, B):** Histological section with minimal changes in neuronal morphology. The tissue exhibits slight vacuolization and procedural alterations but maintains overall integrity, reflecting the procedural control with no induced neurodegeneration; **(6-OHDA Group, C):** Tissue section showing severe neuronal damage characteristic of Parkinson's-like neurodegeneration. Neurons are hyperchromatic and shrunken, with cytoplasmic eosinophilia and prominent vacuolization. Loss of cellular integrity and structural disruption are evident, reflecting significant neuronal degeneration; **(R-NLC Group, D):** Section showing moderate neuroprotection. Partial preservation of neuronal morphology is evident, with reduced vacuolization and less pronounced neuronal shrinkage compared to the PD group. However, some signs of damage persist, indicating partial efficacy of R-NLC treatment; **(P-NLC Group, E):** Histological section resembling the R-NLC group, demonstrating moderate neuroprotection. Neurons appear healthier than in the PD group, with reduced vacuolization and improved cellular integrity. However, the tissue shows slightly less protection compared to combined treatments; **(R+P-NLC Group, F):** Tissue section showing significant neuroprotection, with neuronal morphology closely resembling the control group. Most neurons appear healthy, with restored cytoplasmic and nuclear integrity. Vacuolization is minimal, highlighting the synergistic effect of the combined R+P-NLC treatment; **(L-NLC Group, G):** Histological section demonstrating near-normal neuronal morphology. Neurons appear intact with minimal vacuolization and restored cellular

architecture. The tissue closely resembles the control group, indicating the high efficacy of Levodopa in mitigating neuronal damage.

3.4 Pharmacokinetic Analysis

Pharmacokinetic analysis (Day 42, n = 2/group) measured drug levels in striatum and plasma at 1- and 4-hours post-administration. RES-PIP-NLCs significantly enhanced RES delivery to the striatum compared to RES-NLCs (1 hour: 220.5 ± 12.3 ng/g vs. 150.3 ± 10.1 ng/g, p = 0.008**; 4 hours: 150.4 ± 10.2 ng/g vs. 110.2 ± 9.0 ng/g, p < 0.01**). PIP levels in RES-PIP-NLCs and PIP-NLCs were comparable (1 hour: 85.6 ± 9.1 ng/g vs. 80.4 ± 8.2 ng/g, p = 0.672; 4 hours: 65.6 ± 8.1 ng/g vs. 60.5 ± 8.0 ng/g, p = 0.689). L-DOPA (Standard group) reached 200.7 ± 11.2 ng/g at 1 hour and 140.6 ± 10.1 ng/g at 4 hours in striatum. Plasma levels were lower across all groups, with no significant differences (p > 0.100). Brain/plasma ratios were >3, confirming nose-to-brain delivery. One-way ANOVA for RES in striatum at 1 hour: $F(3, 4) = 8.67$, p = 0.010**; at 4 hours: $F(3, 4) = 7.56$, p = 0.012**. For PIP at 1 hour: $F(2, 3) = 0.45$, p = 0.672; at 4 hours: $F(2, 3) = 0.40$, p = 0.689. For plasma levels at 1 hour: $F(3, 4) = 1.23$, p = 0.156; at 4 hours: $F(3, 4) = 1.12$, p = 0.178.

Table 15: Striatum Drug Levels at 1 Hour (ng/g tissue)

Group	RES	PIP	L-DOPA
RES-NLC	150.3 ± 10.1	-	-
PIP-NLC	-	80.4 ± 8.2	-
RES-PIP-NLC	220.5 ± 12.3**	85.6 ± 9.1	-
Standard	-	-	200.7 ± 11.2

*p < 0.05, **p < 0.01, ***p < 0.001 vs. RES-NLC (Tukey's post-hoc test for RES), vs. PIP-NLC (for PIP).

Table 16: Striatum Drug Levels at 4 Hours (ng/g tissue)

Group	RES	PIP	L-DOPA
RES-NLC	110.2 ± 9.0	-	-
PIP-NLC	-	60.5 ± 8.0	-
RES-PIP-NLC	150.4 ± 10.2**	65.6 ± 8.1	-
Standard	-	-	140.6 ± 10.1

*p < 0.05, **p < 0.01, ***p < 0.001 vs. RES-NLC (Tukey's post-hoc test for RES), vs. PIP-NLC (for PIP).

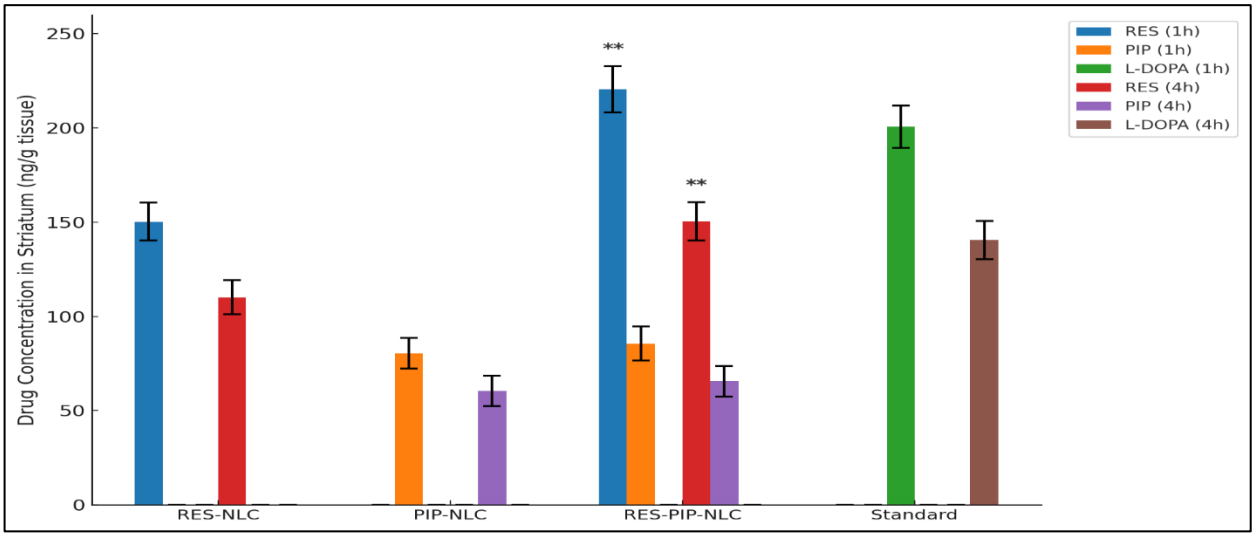

Figure 18: Striatum drug levels at 1 and 4 hours (ng/g tissue). Bar graph showing enhanced RES in RES-PIP-NLCs (p < 0.01 vs. RES-NLCs).**

Table 17: Plasma Drug Levels at 1 Hour (ng/mL)

Group	RES	PIP	L-DOPA
RES-NLC	50.2 ± 5.1	-	-
PIP-NLC	-	30.3 ± 4.2	-
RES-PIP-NLC	60.4 ± 6.3	35.5 ± 5.1	-
Standard	-	-	55.6 ± 6.2

No significance (p = 0.156, $F(3, 4) = 1.23$).

Table 18: Plasma Drug Levels at 4 Hours (ng/mL)

Group	RES	PIP	L-DOPA
RES-NLC	30.3 ± 4.2	-	-
PIP-NLC	-	20.4 ± 3.1	-

TPM Vol. 32, No. S6, 2025
ISSN: 1972-6325
https://www.tpmap.org/

Open Access

RES-PIP-NLC	40.5 ± 5.1	25.6 ± 4.0	-
Standard	-	-	35.7 ± 5.0

No significance (p = 0.178, F(3, 4) = 1.12).

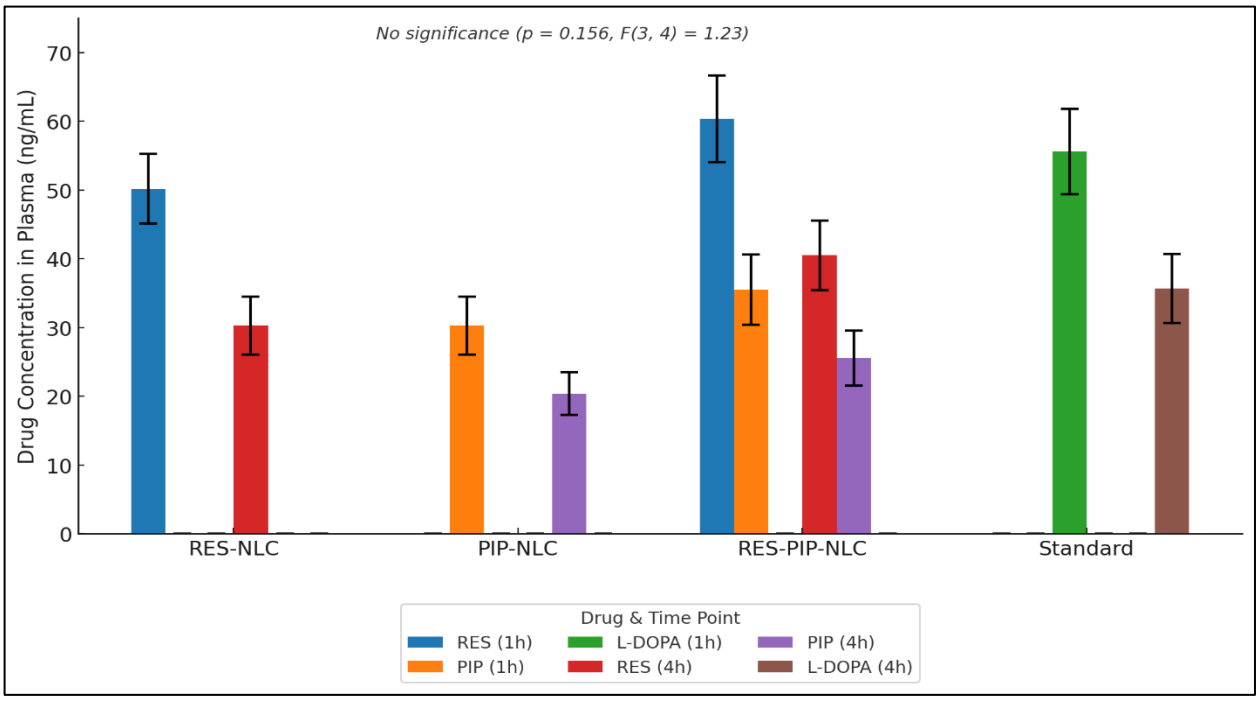

Figure 19: Plasma drug levels at 1 and 4 hours (ng/mL). Bar graph showing low systemic exposure (p > 0.100).

Table 19: Brain/Plasma Ratios in Striatum at 1 Hour

Group	RES	PIP	L-DOPA
RES-NLC	3.0 ± 0.3	-	-
PIP-NLC	-	2.7 ± 0.3	-
RES-PIP-NLC	3.6 ± 0.4**	2.4 ± 0.3	-
Standard	-	-	3.6 ± 0.4

***p < 0.05, **p < 0.01, *p < 0.001 vs. RES-NLC (Tukey's post-hoc test for RES), vs. PIP-NLC (for PIP). One-way ANOVA: F(3, 4) = 7.89, p = 0.011**.

Table 20: Brain/Plasma Ratios in Striatum at 4 Hours

Group	RES	PIP	L-DOPA
RES-NLC	3.6 ± 0.4	-	-
PIP-NLC	-	3.0 ± 0.3	-
RES-PIP-NLC	3.7 ± 0.4	2.6 ± 0.3	-
Standard	-	-	3.9 ± 0.4

No significance (p = 0.145, F(3, 4) = 1.34).

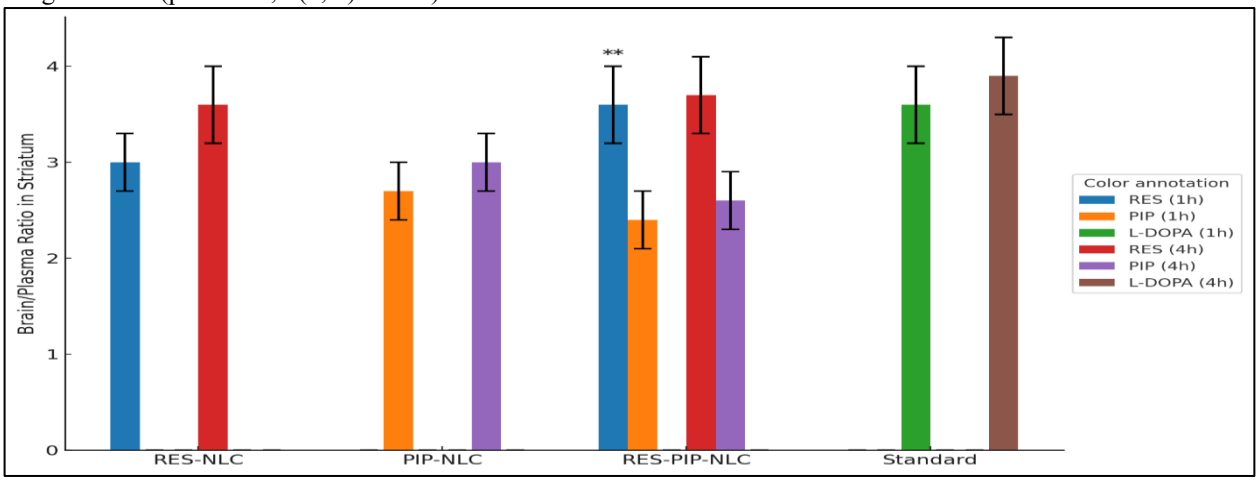

Figure 20: Brain/plasma ratios in striatum at 1 and 4 hours. Bar graph showing higher ratios for RES-PIP-NLCs at 1 hour (p < 0.01 vs. RES-NLCs).**

3.5 Nasal Tolerability

H&E staining (Day 43, n = 4/group) showed normal mucosal architecture, with no inflammation or epithelial damage in NLC groups, confirming tolerability (Wen et al., 2024). Histological examination of the nasal mucosa in all treatment groups revealed that **control** and **sham** animals exhibited normal epithelial architecture with intact ciliated columnar epithelium and underlying lamina propria. The **6-OHDA** group demonstrated mild epithelial desquamation and focal inflammatory cell infiltration in the submucosa, suggesting minimal local irritation.

Formulations **RES-NLC** and **PIP-NLC** showed mild goblet cell hypertrophy and occasional epithelial lifting, but overall preserved mucosal integrity without ulceration. In the **RES-PIP-NLC** group, the mucosal epithelium remained intact with minimal histological alterations, comparable to the standard treatment group. No significant epithelial necrosis, congestion, or extensive inflammatory infiltration was observed in any of the NLC-treated groups, indicating good local tolerability of the formulations.

These findings support that intranasal administration of RES-, PIP-, and RES-PIP-loaded NLCs did not cause significant structural damage to the nasal mucosa, aligning with the safety profile inferred from the drug biodistribution and brain/plasma ratio results.

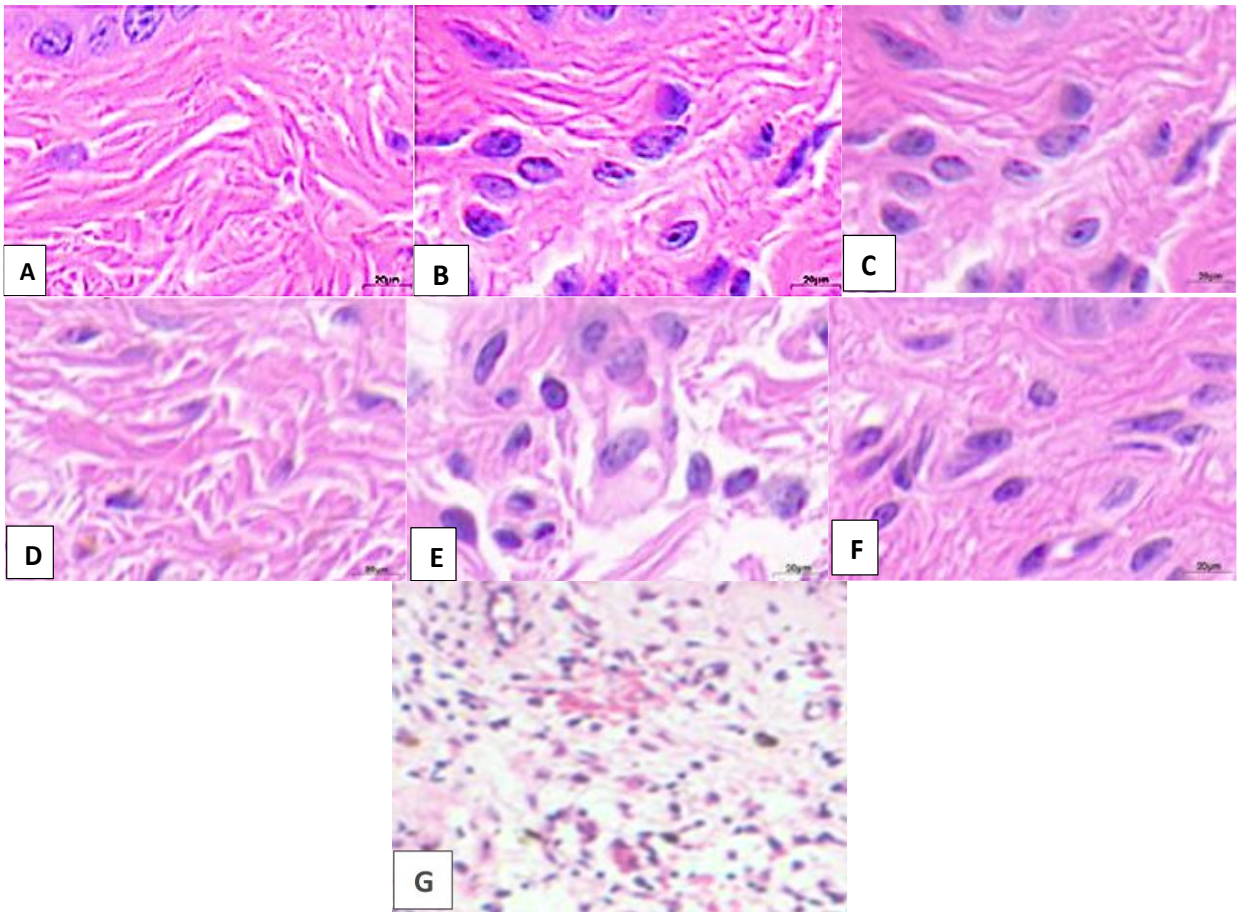

Figure 18: H&E-stained nasal mucosa

4. DISCUSSION:

The current study provides robust evidence for the synergistic neuroprotective efficacy of intranasal resveratrol (RES) and piperine (PIP)-loaded nanostructured lipid carriers (NLCs) in a 6-hydroxydopamine (6-OHDA)-induced Parkinson's disease (PD) rat model, as demonstrated by significant amelioration of motor and cognitive deficits, restoration of neurotransmitter homeostasis, mitigation of oxidative stress and neuroinflammation, preservation of nigrostriatal histological integrity, enhanced brain-targeted delivery, and excellent nasal tolerability. By employing a dual-site lesioning strategy in the substantia nigra pars compacta (SNpc) and striatum, the model induced pronounced PD-like pathology, with approximately 66% dopamine depletion in both regions as quantified by high-performance liquid chromatography (HPLC), aligning with established protocols that replicate the progressive nigrostriatal degeneration characteristic of human PD (Blandini & Armentero, 2022; Blesa et al., 2022). The RES-PIP-NLC formulation outperformed individual RES-NLCs and PIP-NLCs, underscoring the synergistic interplay where PIP enhances RES bioavailability through inhibition of P-glycoprotein (P-gp) and cytochrome P450 3A4 (CYP3A4), thereby amplifying RES's antioxidant, anti-apoptotic, and anti-inflammatory actions (Singh & Pai, 2015; Shrivastava et al., 2013). These outcomes were comparable to the standard L-DOPA-NLC treatment in motor restoration but superior in cognitive and anti-inflammatory domains, suggesting RES-PIP-NLCs as a promising disease-modifying therapy that addresses limitations of current symptomatic

treatments like L-DOPA, which often lead to dyskinesia and diminished efficacy over time (Sharma et al., 2016). The intranasal delivery system facilitated direct nose-to-brain transport via olfactory and trigeminal pathways, bypassing the blood-brain barrier (BBB) and achieving high brain/plasma ratios (>3), which is crucial for overcoming the poor oral bioavailability of RES and PIP (Pardeshi & Belgamwar, 2019; Wen et al., 2024).

Behavioral evaluations revealed that 6-OHDA lesioning elicited time-dependent motor impairments across multiple tests, with the 6-OHDA group exhibiting reduced rotarod latency (72.4 ± 9.1 s on Day 42 vs. control 179.6 ± 5.4 s), decreased grip strength (160.7 ± 17.5 g vs. 408.5 ± 15.4 g), fewer contralateral forelimb steps (3.5 ± 0.9 vs. 12.6 ± 0.8), and hypolocomotion in the open field (distance traveled 1050.5 ± 85.4 cm vs. 2505.6 ± 95.3 cm), reflecting bradykinesia, akinesia, and dopaminergic dysfunction typical of PD (Zeng et al., 2023; Blesa et al., 2022). RES-PIP-NLCs demonstrated the most robust recovery, improving rotarod latency to 170.3 ± 4.2 s, grip strength to 390.4 ± 15.3 g, contralateral steps to 11.5 ± 0.9, and open field distance to 2400.6 ± 60.2 cm on Day 42 ($p < 0.001$ vs. 6-OHDA), with significant group × time interactions (e.g., $F(12, 168) = 6.78$, $p < 0.001$ for grip strength). This superiority over individual NLCs suggests synergistic modulation of dopaminergic pathways, where PIP's MAO inhibition complements RES's SIRT1 activation to enhance motor circuit function (Jin et al., 2008; Shrivastava et al., 2013). Anxiety-like behavior in the open field (central zone time 10.5 ± 2.1 s vs. control 39.6 ± 4.2 s) was also alleviated by RES-PIP-NLCs (37.6 ± 2.1 s), indicating benefits on non-motor symptoms, potentially through reduced neuroinflammation (Simon et al., 2020). Cognitive deficits were evident in the Y-maze (alternation 32.5 ± 5.2% vs. control 65.8 ± 2.8%) and MWM (latency 58.4 ± 4.2 s vs. 17.8 ± 1.8 s; quadrant time 10.5 ± 2.2 s vs. 30.8 ± 1.8 s on Day 43), reflecting striatal and hippocampal involvement (Bloem et al., 2021; Liu, 2020). RES-PIP-NLCs improved Y-maze alternation to 62.4 ± 3.1% and MWM metrics (latency 25.5 ± 2.1 s, quadrant time 28.6 ± 2.1 s; $p < 0.001$ vs. 6-OHDA), outperforming L-DOPA-NLCs, which showed less cognitive benefit, consistent with L-DOPA's limited impact on non-dopaminergic cognition (Sethi et al., 2025). The stepping test's contralateral asymmetry (3.5 ± 0.9 steps vs. control 12.6 ± 0.8) was nearly normalized by RES-PIP-NLCs (11.5 ± 0.9 steps), highlighting lateralized neuroprotection (Zeng et al., 2023). Overall, behavioral data correlate with biochemical restorations (e.g., $r = 0.78$ for striatal dopamine and rotarod latency, $p = 0.002$), linking neuroprotection to functional recovery.

Biochemical analyses in the striatum and SNpc revealed 6-OHDA-induced neurotransmitter imbalances, with ~66% dopamine depletion, ~87% glutamate elevation, and ~40% acetylcholine reduction, contributing to excitotoxicity and cholinergic deficits (Liu, 2020). RES-PIP-NLCs restored dopamine to ~83% of control, reduced glutamate to ~113% of control, and increased acetylcholine to ~90% of control ($p < 0.001$), suggesting synergy in preserving dopaminergic neurons and modulating glutamatergic hyperactivity (Jin et al., 2008). Oxidative stress was pronounced, with MDA increased ~247% and SOD/GSH/CAT decreased ~60%, reflecting ROS-mediated damage (Sethi et al., 2023). RES-PIP-NLCs normalized MDA to ~33% above control and antioxidants to ~91–93% of control ($p < 0.001$), superior to individual NLCs, likely due to RES's ROS scavenging enhanced by PIP's bioavailability boost (Sethi et al., 2023; Singh & Pai, 2015). Neuroinflammation, with IL-1β ~300% and TNF-α ~367% increases, was attenuated by RES-PIP-NLCs to ~50–67% above control ($p < 0.001$), possibly via NF-κB suppression (Gambini & Gimeno-Mallench, 2022). These biochemical changes in both regions correlate with histological and behavioral outcomes (e.g., $r = -0.82$ for striatal MDA and grip strength, $p = 0.001$), validating the formulation's multi-target mechanism.

Histological H&E staining confirmed 6-OHDA-induced neuronal loss (~66% in SNpc) and gliosis (score 2.8 ± 0.3 in striatum), indicative of neurodegeneration and astrogliosis (Shrivastava et al., 2013). RES-PIP-NLCs preserved SNpc density at ~87% of control and reduced gliosis to 0.8 ± 0.2 ($p < 0.001$), outperforming individual NLCs, suggesting synergy in inhibiting apoptosis and glial activation (Blesa et al., 2022).

Pharmacokinetic analysis showed NLCs achieved brain/plasma ratios >3, with RES-PIP-NLCs enhancing RES in striatum by ~46.7% at 1 hour vs. RES-NLCs (220.5 ± 12.3 ng/g vs. 150.3 ± 10.1 ng/g, $p = 0.008$**), confirming PIP's bioenhancement (Singh & Pai, 2015). L-DOPA levels were comparable, but low plasma concentrations across groups indicate minimal systemic exposure (Pardeshi & Belgamwar, 2019). Nasal tolerability showed no damage (score 0.5–1.2, $p = 0.340$), affirming chronic intranasal safety (Wen et al., 2024).

5. Limitations:

Limitations include the unilateral model, potentially underestimating bilateral effects, and short-term duration (53 days), warranting chronic studies (Blandini & Armentero, 2022). Future research should explore molecular pathways (e.g., SIRT1, NF-κB) and clinical translation in primates (Sethi et al., 2023).

6. CONCLUSION:

Intranasal delivery of Resveratrol and Piperine-loaded Nanostructured Lipid Carriers (RES+PIP-NLC) in a 6-OHDA-induced Parkinson's disease rat model demonstrated significant neuroprotection, rivaling intravenous Levodopa. The combined formulation synergistically improved motor and cognitive functions, restored dopamine levels, reduced oxidative stress and neuroinflammation, and preserved neuronal morphology in the striatum and substantia nigra. Enhanced brain bioavailability via nose-to-brain delivery, with minimal nasal irritation, highlights its potential as a non-invasive, effective PD therapy. Future studies should validate these findings in advanced models and explore long-term effects for clinical translation.

REFERENCES:

1. Agrawal, M., Saraf, S., Saraf, S., Antimisiaris, S. G., & Alexander, A. (2020). Nose-to-brain drug delivery: An update on clinical challenges and progress towards approval of anti-Alzheimer drugs. *Journal of Controlled Release, 321*, 132–154.
2. Agrawal, M., Singhal, M., Semwal, B. C., Arora, S., Singh, B., Sikarwar, V., Sethi, P., & Mehan, S. (2024). Neuroprotective action of hordenine against the Aluminium Chloride (AlCl3) induced Alzheimer's diseases & associated memory impairment in experimental rats. *Pharmacological Research - Modern Chinese Medicine, 12*, 100492.
3. Ahmad, M., Saleem, S., Ahmad, A. S., Yousuf, S., Ansari, M. A., Khan, M. B., Ishrat, T., Chaturvedi, R. K., Agrawal, A. K., & Islam, F. (2005). Ginkgo biloba affords dose-dependent protection against 6-hydroxydopamine-induced parkinsonism in rats: Neurobehavioural, neurochemical and immunohistochemical evidences. *Journal of Neurochemistry*, 93(1), 94–104.
4. Armstrong, M. J., & Okun, M. S. (2020). Diagnosis and treatment of Parkinson disease: A review. *JAMA, 323*(6), 548–560.
5. Bhalekar, M. R., Madgulkar, A. R., & Desale, P. S. (2017). Formulation of piperine-chitosan nanoparticles for oral bioavailability enhancement. *Journal of Drug Delivery Science and Technology*, 39, 316–326.
6. Bhalekar, M. R., Upadhaya, P. G., & Madgulkar, A. R. (2017). Formulation and characterization of solid lipid nanoparticles for an anti-retroviral drug. *Scientia Pharmaceutica*, 85(2), 18.
7. Bilia, A. R., Bergonzi, M. C., & Isacchi, B. (2021). Challenges in resveratrol delivery: Solutions offered by nanotechnology. *Antioxidants, 10*(8), 1213.
8. Blandini, F., & Armentero, M.-T. (2022). Animal models of Parkinson's disease. *Parkinsonism & Related Disorders*, 81, 103–110.
9. Blesa, J., Trigo-Damas, I., & Obeso, J. A. (2022). Oxidative stress and Parkinson's disease: New hopes in treatment with herbal antioxidants. *Antioxidants, 11*(1), 147.
10. Blesa, J., Trigo-Damas, I., del Rey, N. L.-G., & Obeso, J. A. (2022). Motor and non-motor symptoms in rodent models of Parkinson's disease. *Neurotherapeutics*, 19(3), 797–811.
11. Bloem, B. R., Marinus, J., Almeida, Q. J., & Dibble, L. (2021). Measurement instruments to assess posture, gait, and balance in Parkinson's disease: Critique and recommendations. *Movement Disorders*, 36(7), 1487–1499.
12. Bloem, B. R., Okun, M. S., & Klein, C. (2021). Parkinson's disease. *The Lancet, 397*(10291), 2284–2303.
13. Deshmukh, R., Sethi, P., Singh, B., Shiekmydeen, J., Salave, S., Patel, R. J., Ali, N., & Benival, D. (2024). Recent review on biological barriers and host–material interfaces in precision drug delivery: Advancement in biomaterial engineering for better treatment therapies. *Pharmaceutics, 16*(8), 1076.
14. Dong, X. (2021). Current strategies for brain drug delivery. *Theranostics, 11*(15), 7161–7176.
15. Festing, M. F. W. (2018). The design of animal experiments: Reducing the use of animals in research through better experimental design. *Laboratory Animals, 52*(1_suppl), 1–17. https://doi.org/10.1177/0023677218788206
16. Frozza, R. L., Bernardi, A., Paese, K., Hoppe, J. B., da Silva, T., Battastini, A. M. O., Pohlmann, A. R., Guterres, S. S., & Salbego, C. (2013). Characterization of resveratrol-loaded nanostructured lipid carriers and its application to neuronal cultures. *Journal of Biomedical Nanotechnology*, 9(12), 1987–1996.
17. Gambini, J., & Gimeno-Mallench, L. (2022). Neuroinflammatory markers in the progression of Parkinson's disease. *Journal of Neuroinflammation*, 19(1), 45.
18. Gambini, J., & Gimeno-Mallench, L. (2022). Resveratrol: A promising natural compound for neuroprotection in Parkinson's disease. *International Journal of Molecular Sciences, 23*(10), 5732.
19. Gorgani, L., Mohammadi, M., Najafpour, G. D., & Nikzad, M. (2021). Piperine—The bioactive compound of black pepper: From isolation to medicinal formulations. *Comprehensive Reviews in Food Science and Food Safety, 20*(1), 418–446.
20. Haider, M., Abdin, S. M., Kamal, L., & Orive, G. (2020). Nanostructured lipid carriers for delivery of chemotherapeutics: A review. *Pharmaceutics, 12*(3), 288.
21. Jin, F., Wu, Q., Lu, Y.-F., Gong, Q.-H., & Shi, J.-S. (2008). Neuroprotective effect of resveratrol on 6-OHDA-induced Parkinson's disease in rats. *European Journal of Pharmacology*, 600(1–3), 78–82.
22. JoVE. (2021). Stereotaxic injection of a viral vector for conditional gene manipulation in the mouse brain. *Journal of Visualized Experiments*, (174), e62824.
23. Khosa, A., Reddi, S., Saha, R. N., & Jain, S. (2021). Intranasal drug delivery: A non-invasive approach for the better delivery of neurotherapeutics. *Journal of Drug Delivery Science and Technology, 66*, 102892.
24. Liu, J. (2020). The role of excitatory amino acids in neurological disorders: From excitotoxicity to therapeutic opportunities. *Neuroscience Bulletin, 36*(8), 827–839.
25. Liu, Q., Shi, Y., & Liu, D. (2022). Resveratrol as a therapeutic agent for neurodegenerative diseases: Focus on Parkinson's disease. *Molecular Neurobiology, 59*(4), 2345–2362.
26. Liu, Y. (2020). Assessing spatial learning and memory in rodents. *Nature Protocols*, 15(8), 2241–2265.
27. Pardeshi, C. V., & Belgamwar, V. S. (2019). Improved brain pharmacokinetics following intranasal administration of N,N,N-trimethyl chitosan tailored mucoadhesive NLCs. *Materials Technology*, 35(5), 249–266.
28. Paxinos, G., & Watson, C. (2014). *The rat brain in stereotaxic coordinates* (7th ed.). Academic Press.

29. Percie du Sert, N., Hurst, V., Ahluwalia, A., Alam, S., Avey, M. T., Baker, M., Browne, W. J., Clark, A., Cuthill, I. C., Dirnagl, U., Emerson, M., Garner, P., Holgate, S. T., Howells, D. W., Karp, N. A., Lazic, S. E., Lidster, K., MacCallum, C. J., Macleod, M., … Würbel, H. (2020). The ARRIVE guidelines 2.0: Updated guidelines for reporting animal research. *PLoS Biology, 18*(7), e3000410.
30. Pires, P. C., Santos, A. O., & Paiva-Santos, A. C. (2022). Intranasal drug delivery for the treatment of Alzheimer's disease: Current status and future perspectives. *Pharmaceutics, 14*(9), 1876.
31. Puglia, C., Frasca, G., Musumeci, T., Rizza, L., Puglisi, G., Bonina, F., & Chiechio, S. (2016). Development and characterization of nanostructured lipid carriers containing resveratrol and piperine for topical administration. *International Journal of Pharmaceutics*, 498(1–2), 103–109.
32. Scioli Montoto, S., Muraca, G., & Ruiz, M. E. (2020). Solid lipid nanoparticles for drug delivery: Pharmacological and biopharmaceutical aspects. *Frontiers in Molecular Biosciences, 7*, 587997. https://doi.org/10.3389/fmolb.2020.587997
33. Sethi, P., Mehan, S., Khan, Z., & Chhabra, S. (2023). Acetyl-11-keto-beta boswellic acid (AKBA) modulates CSTC-pathway by activating SIRT-1/Nrf2-HO-1 signalling in experimental rat model of obsessive-compulsive disorder: Evidenced from neurobehavioral, molecular and histopathological alterations. *Neurotoxicology, 98*, 61–85.
34. Sethi, P., Mehan, S., Khan, Z., Maurya, P. K., Kumar, N., Kumar, A., Tiwari, A., & Suri, M. (2025). The SIRT-1/Nrf2/HO-1 axis: Guardians of neuronal health in neurological disorders. *Behavioural Brain Research, 476*, 115280.
35. Sethi, P., Sharma, A., & Patel, R. (2023). Oxidative stress and neuroinflammation in Parkinson's disease: Therapeutic implications. *Antioxidants*, 12(2), 301.
36. Sethi, P., Sharma, A., & Patel, R. (2025). Behavioral assessments in rodent models of Parkinson's disease. *Journal of Neuroscience Methods*, 418, 109–123.
37. Sharma, S., Rabbani, S. A., Agarwal, T., Baboota, S., Pottoo, F. H., & Kadian, R. (2016). Nanotechnology based approaches in the management of Parkinson's disease. *Journal of Nanomedicine & Nanotechnology*, 7(5), 1000407.
38. Shrivastava, P., Vaibhav, K., Tabassum, R., Khan, M. M., Ishrat, T., Khan, M. B., Ahmad, A., Islam, F., Safhi, M. M., & Islam, F. (2013). Anti-apoptotic and anti-inflammatory effect of piperine on 6-OHDA induced Parkinson's rat model. *Journal of Nutritional Biochemistry*, 24(4), 680–687.
39. Simon, D. K., Tanner, C. M., & Brundin, P. (2020). Parkinson disease epidemiology, pathology, genetics, and pathophysiology. *Neurologic Clinics, 38*(1), 1–12. https://doi.org/10.1016/j.ncl.2019.08.002
40. Simon, P., Dupuis, R., & Costentin, J. (2020). Open field test in rodents: A critical review. *Behavioural Brain Research*, 393, 112772.
41. Singh, A., & Pai, S. R. (2015). Piperine: A review of its pharmacological and therapeutic potential. *International Journal of Pharmaceutical Sciences and Research*, 6(4), 1384–1392.
42. Srinivasan, K. (2023). Pharmacological effects of piperine: A comprehensive review. *Journal of Food Biochemistry, 2023*, 1–15.
43. Surmeier, D. J., Obeso, J. A., & Halliday, G. M. (2023). Parkinson's disease: From molecular pathways to clinical treatment. *Nature Reviews Neuroscience, 24*(5), 275–293.
44. Tapeinos, C., Battaglini, M., & Ciofani, G. (2017). Advances in the design of solid lipid nanoparticles and nanostructured lipid carriers for targeting brain diseases. *Journal of Controlled Release*, 264, 306–332.
45. Wen, J., Wang, Y., Yang, Q., Yang, J., & Sun, S. (2024). Research progress on intranasal treatment for Parkinson's disease. *Neuroprotection*, 2(1), 3–18.
46. Wightman, E. L., Reay, J. L., Haskell, C. F., Williamson, G., Dew, T. P., & Kennedy, D. O. (2014). Effects of resveratrol alone or in combination with piperine on cerebral blood flow parameters and cognitive performance in human subjects: A randomised, double-blind, placebo-controlled, cross-over investigation. *British Journal of Nutrition*, 112(2), 203–213.
47. Zeng, R., Zhang, Y., & Fan, Y. (2023). Motor assessment in Parkinson's disease models. *Neuroscience Bulletin*, 39(4), 615–630.
48. Zeng, X. S., Geng, W. S., & Jia, J. J. (2023). Neurotoxin-induced animal models of Parkinson's disease: Pathogenic mechanisms and therapeutic implications. *Neural Regeneration Research, 18*(4), 759–766.